JCI The Journal of Clinical Investigation

Exosomal TNF-α mediates voltage-gated Na^+ channels 1.6 overexpression and contributes to brain-tumor induced neuronal hyperexcitability

Cesar Adolfo Sanchez Trivino, … , Fabrizia Cesca, Vincent Torre

J Clin Invest. 2024. https://doi.org/10.1172/JCI166271.

Research In-Press Preview **Neuroscience** **Oncology**

Patients affected by glioma frequently suffer of epileptic discharges, however the causes of brain tumor-related epilepsy (BTRE) are still not completely understood. We investigated the mechanisms underlying BTRE by analyzing the effects of exosomes released by U87 glioma cells and by patient-derived glioma cells. Rat hippocampal neurons incubated for 24 h with these exosomes exhibited increased spontaneous firing, while their resting membrane potential shifted positively by 10-15 mV. Voltage clamp recordings demonstrated that the activation of the Na^+ current shifted towards more hyperpolarized voltages by 10-15 mV. To understand the factors inducing hyperexcitability we focused on exosomal cytokines. Western Blot and ELISA assays show that TNF-α is present inside glioma-derived exosomes. Remarkably, incubation with TNF-α fully mimicked the phenotype induced by exosomes, with neurons firing continuously, while their resting membrane potential shifted positively. RT-PCR revealed that both exosomes and TNF-α induced over-expression of the voltage-gated Na channel Nav1.6, a low-threshold Na^+ channel responsible for hyperexcitability. When neurons were preincubated with Infliximab, a specific TNF-α inhibitor, the hyperexcitability induced by exosomes and TNF-α were drastically reduced. We propose that Infliximab, an FDA approved drug to treat rheumatoid arthritis, could ameliorate the conditions of glioma patients suffering of BTRE.

Exosomal TNF-α mediates voltage-gated Na^+ channels 1.6 overexpression and contributes to brain-tumor induced neuronal hyperexcitability

Cesar Adolfo Sanchez Trivino[1], Renza Spelat[1,2]*, Federica Spada[1,3], Camilla D'Angelo[1], Ivana Manini[4], Irene Giulia Rolle[4], Tamara Ius[5], Pietro Parisse[2], Anna Menini[1], Daniela Cesselli[4], Miran Skrap[6], Fabrizia Cesca[3+], Vincent Torre[1,2,7,8+]*

[1]*International School for Advanced Studies (SISSA), via Bonomea 265, Trieste, Italy*

[2]*Institute of Materials (IOM-CNR), Area Science Park, Basovizza, Trieste, Italy*

[3]*Department of Life Sciences, University of Trieste, Italy*

[4]*Università degli studi di Udine, Istituto di Anatomia Patologica, ASUIUD, Italy*

[5]*Neurosurgery Unit, Department of Neurosciences, Santa Maria della Misericordia University Hospital, Udine, Italy*

[6]*SOC Neurochirurgia, Az. Ospedaliera Sanitaria Integrata, Udine, Italy*

[7]*BISS GlioGuard S.r.l., Trieste, Italy*

[8]*Suzhou Institute of Nano-Tech and Nano-Bionics, Chinese Academy of Sciences, Jiangsu, P.R. China*

**equally contributed*

[+]*corresponding authors':*

Vincent Torre: Institute of Materials (IOM-CNR), Area Science Park, Basovizza, 34149 Trieste, Italy

Ph: +39 333 228 8515

torre@sissa.it,

Fabrizia Cesca*:* Department of Life Sciences, University of Trieste, 34127 Italy

Ph. +39 040 558 8727

fcesca@units.it

Running head: Glioma exosomes induce neural hyperexcitablity

The authors have declared that no conflict of interest exists.

Abstract

Patients affected by glioma frequently suffer of epileptic discharges, however the causes of brain tumor-related epilepsy (BTRE) are still not completely understood. We investigated the mechanisms underlying BTRE by analyzing the effects of exosomes released by U87 glioma cells and by patient-derived glioma cells. Rat hippocampal neurons incubated for 24 h with these exosomes exhibited increased spontaneous firing, while their resting membrane potential shifted positively by 10-15 mV. Voltage clamp recordings demonstrated that the activation of the Na^+ current shifted towards more hyperpolarized voltages by 10-15 mV. To understand the factors inducing hyperexcitability we focused on exosomal cytokines. Western Blot and ELISA assays show that TNF-α is present inside glioma-derived exosomes. Remarkably, incubation with TNF-α fully mimicked the phenotype induced by exosomes, with neurons firing continuously, while their resting membrane potential shifted positively. RT-PCR revealed that both exosomes and TNF-α induced over-expression of the voltage-gated Na channel Nav1.6, a low-threshold Na^+ channel responsible for hyperexcitability. When neurons were preincubated with Infliximab, a specific TNF-α inhibitor, the hyperexcitability induced by exosomes and TNF-α were drastically reduced. We propose that Infliximab, an FDA approved drug to treat rheumatoid arthritis, could ameliorate the conditions of glioma patients suffering of BTRE.

Keywords: brain-tumor related epilepsy (BTRE), glioma-derived exosomes, voltage-gated sodium channel 1.6 (Nav1.6), tumor necrosis factor alpha (TNFα), infliximab.

Introduction

Patients with brain tumors develop symptoms ranging from headaches to epileptic discharges to impairment of specific cognitive functions (1–3). The mechanisms leading to brain tumor related epilepsy (BTRE) are not completely understood and it is thought to have multiple origins (4, 5). The main causes of BTRE are ascribed to tumor growth, disruption of the blood brain barrier, altered synaptic functions and pathologies of the communication between neurons and other brain cells. BTRE is certainly caused by the growth of the tumor and the associated unusual pressure on the healthy tissue but can also be caused by the release of specific factors from tumor cells. Glioma release several factors in the microenvironment; amongst these factors are extracellular vesicles (EVs), including exosomes (6, 7), which contain a large variety of molecules, including proteins, in particular cytokines, and small RNAs (8–13). EVs are released by all cells and regulate intercellular communication both in health and disease conditions (14). EVs thus play a crucial role in tumor growth, invasion, metastasis, angiogenesis and immunity and mediate critical communication between the tumor cells and their microenvironment to sustain the glioma. Glioma-derived EVs deliver unique cargoes such as proteins, nucleic acids and lipids to recipient cells, to alter their gene expression profile and phenotypes (15).

Cancer stem cells in glioma have been described by several studies (16–18). Glioma stem cells (GSCs) are shielded in a particular niche, where factors are released in order to maintain their state (19–22). Glioma-associated stem cells (GASCs) are a population of stem cells representative of the tumor microenvironment. GASCs are present in gliomas and, although not tumorigenic, they support the aggressiveness of GSCs. Moreover, GASCs influence different processes such as tumor progression, cell deformability and interactions with GSCs (23, 24). The release of exosomes contribute to the tumor-supporting features of GASCs, being able to increase proliferation, motility and anchorage independent growth of GSCs (23). Furthermore, SEMA7A carried by GASC-derived exosomes enhances the motility of GSCs, via interaction with β1-integrin, expressed on GSCs surface (25). We recently showed that

exosomes released from GASCs induce a massive cross talk between tumor and neurons inducing a global alteration of network activity (26).

In the present manuscript we studied the effect of glioma-derived exosomes on the firing properties of primary rodent neurons, with the aim of getting more insights into the molecular mechanisms inducing BTRE. We used exosomes secreted by U87 cells and by glioma-derived cells obtained from patients who underwent surgery. Our findings can be summarized as follows: (i) Both cells' and patients' exosomes induced an increase of spontaneous firing; (ii) Exosomes contain the cytokine Tumor Necrosis Factor-alpha (TNF-α), which induces an almost steady and spontaneous firing in healthy cerebral neurons (27–29); (iii) A detailed analysis of the biophysical properties of the voltage gated currents revealed that both exosomes and TNF-α shift the activation of Na^+ currents towards more negative voltages and, as a consequence, neurons are hyperexcitable and fire continuously; (iv) Infliximab, an FDA approved drug (30), reduces the heightened firing induced in vitro by exosomes and by TNF-α. This result can be applicable in the clinical setting by bridging the knowhow of neurosurgeons with those of neurobiologists. Infliximab is expected to ameliorate the conditions of patients with glioma suffering from epileptic seizures.

Results

U87 and patients' exosomes induce increased spontaneus firing in primary neurons

Exosomes were isolated from the conditioned medium of patient-derived GSCs and GASCs (23, 25, 31) and characterized by nanoparticle tracking analysis to define size and concentration. To confirm the identity of isolated particles, the expression of specific exosomal markers such as Flotillin1, Tumor susceptibility gene 101 (TSG-101), and Programmed cell death 6 interacting protein (Alix) was assessed (26). Atomic Force Microscopy was utilized to visualize isolated exosomes, while in the control samples only smaller particles were identified, probably residues of the isolation procedure (Supplemental Figure 1A). Isolated vesicles revealed a diameter of about 130 nm (Supplemental Figure 1B), as expected for small/medium extracellular vesicles (23, 32, 33).

Dissociated hippocampal neurons at DIV 8-15 (in few experiments also cortical neurons, as detailed), were incubated for 24 h with 4.2 x 10^3 U87 exosome per neuron, and the electrical properties before and after incubation were compared. No estimation of exosome concentration in the peritumoral tissue is available in the literature, likely because of the many variables involved. For our experiments we used exosome concentrations of 30 µg/mL, in line with (34)(1–100 µg/mL) and references therein: 30 µg/mL (35), 50 µg/mL (36), and lower than what used in primary MN cultures (37), i.e., 5×10^5 particles/cell (our concentration: 2.1-4.2x10^3 particles/cell), indicating that we are operating within a low-medium range of exosome concentration.

In all experiments, control samples were treated with nanoparticles obtained from culture medium which did not come into contact with cells, subjected to the same exosome isolation procedure. Additional control groups were performed in some experiments and are described where pertinent. Current clamp recordings of control neurons (black traces and symbols in Figure 1, A-C) showed a resting membrane potential (RMP) of -63.5 +/- 2 mV (n=16), action potential (AP) threshold at -40 +/- 1.4 mV (n=16) and a firing pattern in bursts with a mean AP frequency of 0.98 ± 0.2 Hz (38–40). In contrast, neurons incubated with U87 exosomes had a more depolarized RMP of -48.8 +/- 1.15 mV (n=22) and fired spontaneously (2.05 ± 0.38 Hz;

blue traces and symbols in Figure 1, A-C). Increased excitability was not seen following incubation with exosomes deriving from healthy human astrocytes (HA), an additional control group (Figure 2). To investigate whether exosome exposure had any adverse effect on neurons, resulting in an injury discharge and a consequent increased firing, we computed the distribution of AP voltage peak in control and treated neurons finding that 90% of the values were distributed in the range between +10 and +50 mV (Figure 1D). In addition, the mean values of the AP peak in both experimental groups were comparable (treated neurons 32.7 ± 1 mV and control 33.1 ± 0.94 mV, Figure S2). Current clamp recordings show that control neurons exhibited spontaneous bursts of APs and had clear synaptic input. Neurons firing more vigorously had also larger synaptic currents, as evidenced by the voltage clamp recordings at -70 mV (Figure 1, E-G, black traces), and as previously reported (41–45). Conversely, the spontaneous firing of neurons preincubated with exosomes was almost independent of the amount and frequency of synaptic currents; indeed, the higher AP activity of treated neurons was observed both in the presence and in the absence of strong synaptic inputs (Figure 1, E-H, blue traces).

We performed similar experiments with GSC and GASC exosomesfrom 8 patients (Supplemental Table 1). Rodent hippocampal neurons were treated with these exosomes, at the same concentration as in previous experiments. Collected data show that the average RMP of neurons treated with patients' exosomes varied between -42.8 (S496) and -57.7 (S226) mV, more depolarised than untreated neurons, whose average values varied between -59.2 and -76.8 mV (Figure 2, A-B, Supplemental Table 2). Moreover, treated neurons had a more vigorous spontaneous activity, with the exception of patients #S58 and #S226. The firing frequency (Figure 2, A and C) of treated neurons shows average values between 3.19 (S471) and 1.58 Hz (S226), higher than that of control neurons (1.46 to 0.13 Hz, Supplemental Table 3). The effect of exosomes from different patients was variable and we could not make a correlation with their clinical history, which was not available to us. However, we had access to a short clinical summary and we noted that exosomes from patients with severe epileptic

episodes (GSC-#S496 and GASC-#S479) induced a more depolarized shift of the RMP and more intense firing. The RMP and the firing frequency of neurons treated with exosomes from HA (pink traces and symbols) were -65.4 ± 2.7 mV and 0.16 ± 0.08 Hz respectively, similar to those of control neurons. Description of the statistical significance for different patients is reported in Figure 2 legend. For some patients we had limited amount of material, sufficient for few experiments. However, even samples with low numerosity show low variability, and in addition data obtained with exosomes derived from different patients are consistent, supporting our conclusions. The effect of exosomes on cortical neurons was more variable than in hippocampal neurons (Supplemental Figure 3), possibly due to the greater heterogenity of cortical neurons (46).

The effect of patient-derived exosomes depends on the brain region from which they are derived

To better examine the impact of patient exosomes, we investigated whether the observed results could be influenced by the brain region from which they originated. We collaborated with neurosurgeons and neurologists performing electroencephalographic measurements during surgery. During a surgery of a brain solid tumor, four samples from different brain areas were obtained (Figure 3, A-D). These fragments were dissociated, GSCs were cultured, and secreted exosomes harvested. Exosomes from a fragment classified as a Grade IV malignant glioblastoma induced heightened firing in hippocampal neurons, with increased firing rate (Figure 3C). In contrast, exosomes from GSCs from Low Grade fragments did not elicit such behavior (Figure 3, A,B and D). Of note, we observed a trend shift in the RMP toward more positive values, which reached statistical significance for the temporal and parietal fragments, in agreement with our previous data. These results suggest that the effect of exosomes depends on both the cortical area from which they derived and the degree of the tumor, consistent with our previous observations (47), highlighting the complexity of BTRE and of exosome action.

Exosomes increase neuronal excitability independently of the cellular type, accelerating the depolarizing phase of action potential initiation.

We then investigated whether the exosome effects differed depending on hippocampal neuron morphology (48). We loaded the solution filling the patch electrodes with fluorescein (49) to distinguish neurons with a bipolar or pyramidal morphology (50–52)(Supplemental Figure 4, A and B). The results evidenced that both bipolar and pyramidal neurons treated with exosomes increased their spontaneous firing and had a more depolarized RMP (Supplemental Figure 4B).

Then, we plotted the spontaneous firing activity measured in current-clamp (I=0) against the synaptic input (measured in voltage-clamp at -80 mV) for each cell, searching for any evidence of coupling between the activity of these neurons within the network (Supplemental Figure 4, C and D). As expected, control neurons exhibited a positive correlation with synaptic input (r^2=0.72). In contrast, in exosome-treated neurons AP firing became independent of synaptic activity (Supplemental Figure 4D). Next, we compared pyramidal neurons with high spontaneous activity (Supplemental Figure 4E), quantifying their GABAergic and glutamatergic events, based on their characteristic decay time constants. We found that AP firing in these cells was independent of GABA input (Supplemental Figure 4, F and G), with no evident correlation between GABA input frequency (Supplemental Figure 4H). This suggests that exosomes might disproportionately affect GABAergic cells, rendering their synaptic input silent and incapable of counteracting the increased excitability of pyramidal neurons.

We also verified that neurons, when injected with hyperpolarizing currents (-10 to -70 pA) bringing their RMP close to -70 mV, i.e. approximately the value of control neurons, decreased their firing frequency which approached that of untreated neurons. Of note, the same procedure did not elicit any change in frequency in control neurons (Figure 4, A and B). Moreover, the analysis of the AP phase plot, i.e. dV/dt versus V, revealed that treated neurons held at -70 mV for 100 ms exhibited a significant increase in the maximum depolarization rate

(dV/dt), as compared to control neurons. In contrast, the control group did not display significant changes of the dV/dt versus V plot when the cells were held at -70 mV (Figure 4, C and D).

Concentration-dependent effect of exosome treatment

We incubated hippocampal neurons with exosomes from patient #S479 at two concentrations: that used for all previous experiments (4.2x10^3 particles/neuron) and half (2.1x10^3 particles/neuron). Under these conditions, the RMP progressively shifted to more depolarized values, i.e. -46.5±4.2 mV for the low concentration and -37.3±1.76 mV for the high concentration, as compared to the control value of -57±2.34 mV (gray and light blue traces and points, Supplemental Figure 5, A and B). Subsequently, in voltage clamp experiments we determined the initial voltage evoking an inward current (FV-IC), which also showed a concentration-dependent shift toward more negative values: -42.2±1.8 mV for the low concentration and -55.3±0.66 mV for the high concentration, compared to control neurons (-37.6±2.1 mV).

In treated neurons (both low and high concentration) FV-IC almost coincided with the RMP of the same cells, consistent with the observed increase of spontaneous AP frequency. For the high-concentration neurons, the FV-IC was more hyperpolarized than the RMP, and neurons either fired almost continuously (pink traces in Fig. S5A) or were unable to generate spontaneous AP, most likely due to the inactivation of the inward current (Supplemental Figure 6A), as further studied in Fig. 5. However, hyperpolarization of the same cells induced firing, confirming the increase in intrinsic excitability (Supplemental Figure 6, B and C).These findings indicate that the effect of exosomes is concentration-dependent and that exposure to exosomes primarily modifies the voltage-gated conductance responsible for spike initiation.

Voltage-gated sodium currents are altered by patient-derived exosomes

In order to collect voltage clamp data with an acceptable spatial clamp, we impaled neurons with a small cell body and limited dendritic harborization. Given an access resistance of 3-5

MΩ, a peak inward Na^+ current of 5 nA implies an error of 15-25 mV, which is not acceptable. If the Na^+ current, in contrast, does not exceed 0.5-1 nA, the error is less than 3 mV, which becomes acceptable. The holding potential was -70 mV, which was briefly moved to -110 mV and then to more positive values according to the planned experiment. In the experiments aimed to determine the activation threshold of the Na^+ current, the voltage was moved up to -20 mV in steps of 2 mV (Figure 5A). We compared data obtained with 140 and 70 mM Na^+ in the extracellular solution (traces in Figure 5A). After normalization to the maximal recorded current, the activation curves of Na^+ current under normal and low Na^+ conditions were almost identical (Figure 5B), and the inward Na^+ current becomes visible at voltages above -45 mV. In the experiments to establish the full range of the inward current activation, the maximum voltage was +40 mV and, in the presence of 70 mM Na^+ in the extracellular solution, the maximal recorded current was in the range of 500 pA (black traces in Figure 5C).

The inward current responsible for the increased spontaneous firing of neurons treated with exosomes could be carried by the entry of Na^+ and/or Ca^{2+} ions. In particular, hippocampal neurons have large voltage-gated Na^+ currents (Nav) (53, 54). To establish the ionic identity of this current, we recorded inward currents with an intracellular solution containing Cs^+ to block outward K^+ currents and extracellular application of Cd^{2+} to block voltage-gated Ca^{2+} channels (Figure 5C). When Na^+ was entirely replaced by N-methyl-d-glucamine (NMDG), the inward current was drastically reduced (Figure 5C, orange traces) and completely abolished upon addition of 100 mM Cd^{2+} (Figure 5C, brown traces). These results indicate that the inward current is almost entirely carried by Na^+ ions, but some Ca^{2+} channels are also present and are activated at positive voltages.

We then compared Na^+ current activation and inactivation in control and treated neurons (Figure 5D) using the appropriate protocols (55, 56). The maximal amplitude of the Na^+ current density in treated neurons was -13.4±1.5 pA/pF (n=14), larger than in control neurons (-7.7±1.6 pA/pF n=10, Figure 5E). The Na^+ current of treated neurons was half activated ($V_{1/2}$) at -37.6±2 mV, about -6.4 mV more negative than control neurons (Figure 5, E and F**,** $V_{1/2}$ -30 ± 1.7 mV). In contrast, Na^+ current inactivation remained unaltered (Figure 5F**,** -46.3 ± 1.5 mV

and -48.4 ± 1.6 mV, respectively). Similarly, patients' exosomes induced a hyperpolarized shift of $V_{1/2}$ from -32±3.4 mV in control cells to -42.3±4.2 mV when treated with GASC-S479 and -42±3.8 mV when treated with GSC-S471. Moreover, average I-V curves of Na^+ currents showed a higher Na^+ current density in cells treated with patients' exosomes compared to the control group: -10.9±1.7 pA/pF for controls, -20.5±2.8 pA/pF for S479, -17.7±1.2 pA/pF for S471 (Figure 5, G and I). When Nav channels are activated by a strong depolarization, a small fraction, typically around 1%, do not inactivate and remain open originating a noninactivating persistent Na^+ current (57). These Na^+ channels are the substrate of the persistent current which could contribute to hyperexcitation of neurons and to epilepsy (58, 59). We attempted to isolate and compare the persistent current in control and treated neurons applying a depolarized ramp with a rate of 0.018 mV/ms, from a holding potential of -100 mV up to -20 mV (Supplemental Figure 7A). To subtract the leakage and obtain only the persistent currents, we used the specific inhibitor Riluzole (58) at 10 μM. Our experiments show the presence of a persistent current in both control and treated neurons with a significantly different activation: application of a Boltzmann equation shows a negative shift of 10.32 mV in treated neurons (Supplemental Figure 7, B and C), in agreement with the shift of the transient Na^+ current (Fig. 5).

Exosomal TNF-α modulates neuronal Na^+ channels

Glioma exosomes contain a large amount of proteins and small RNAs (60, 61). On the basis of previous studies, we focused on cytokines (62, 63). The most abundant cytokines in exosomes are Interleukins (ILs), in particular IL-1, IL-6 and TNF-α. IL-1β and IL-6 preferentially inhibit or decrease Na^+ currents (64, 65), whileTNF-α positively modulates Na^+ currents in peripheral and central neurons (28, 66, 67).

We compared TNF-α expression in U87 and HA exosomes by western blot analysis, using the exosome marker ALIX as loading control (68, 69). The results evidenced a higher expression in U87 exosomes (Figure 6A), suggesting that the increased neuronal excitability

is only induced by high levels of exosomal TNF-α. We also confirmed the presence of TNF-α in patients' exosomes by ELISA (Figure 6B). Next, we compared the expression of Nav channels in hippocampal neurons after 24 h treatment with exosomes and 10 ng/nl TNF-α by Real Time-PCR (RT-PCR). TNF-α induces Nav1.6 and Nav1.7 expression in DRGs (67) and in cortical neurons (66). Nav1.6 are the most abundant Na^+ channels in the human brain and have a low-threshold for spike initiation, while Nav1.2 have a much higher threshold (70). Nav1.4 and Nav1.5 are primarily expressed in muscles and heart (71), Nav1.8 in neurons of the peripheral nervous system (72). Nav1.1 and Nav1.3 are expressed in hippocampal neurons and are involved in the induction of hyperexcitability (73, 74). Therefore, we focused on Nav1.1, Nav1.2, Nav1.3, Nav1.6 and Nav1.7 as potential candidates. RT-PCR experiments showed that U87 exosomes induced Nav1.6 overexpression and had a negligible effect on Nav1.1, Nav1.2, Na1.3 and Nav1.7. TNF-α treatment induced a significant up-regulation of Nav1.6 and Nav1.7 (Figure 6, C and G). Importantly, the increased expression of Nav1.6 was also observed in neurons treated with exosomes from patient #S496 (Figure 6H). Inhibitors of TNF-α are used to treat rheumatoid arthritis and are blockers of TNFR1 and TNFR2. These inhibitors are based on a Fragment of antibody (Fab) targeted to the binding domain of TNFR1/2 to TNF-α and their clinical names are Remicade/Infliximab, Flixabi and Remsima (30). To verify whether TNF-α selectively enhances Nav1.6 expression, neuronal cultures were pre-incubated with 2.5 μg/ml Infliximab for 2 h and then treated with exosomes or TNF-α. Interestingly, pre-treatment with infliximab significantly reduced Nav1.6 overexpression induced by exosomes and TNF-α (Figure 6, C and H).

To further support these results, we treated neurons with U87- and patient-derived exosomes and performed immunofluorescence experiments with anti-Nav1.6 antibodies, followed by quantitative fluorescence analysis of Nav1.6 expression (Figure 6, I and J). We observed increased Nav1.6 fluorescence intensity in neurons treated with U87 and patient S496 exosomes, consistent with the RT-PCR data. Of note, there was no increase in Nav1.6 fluorescence intensity in neurons treated with exosomes from S58 patient, in line with the

electrophysiological data in Fig. 2. Overall, these results indicate that the increased expression of Nav1.6 is the key factor of the hyperexcitability observed in neurons treated with U87 and patients' exosomes.

To confirm the role of Nav1.6 , we investigated the effects of the specific Nav1.6 blocker Zandatrigine (NBI-921352) (75). In treated neurons exhibiting a significant spontaneous firing, the progressive addition of Zandatrigine hyperpolarized the RMP and abolished the spontaneous firing (Figure 6, K and L). When the blocker was removed from the extracellular medium, the RMP moved back to more depolarized values and the original spontaneous firing partially recovered. Conversely, Zandatrigine had only a small effect when applied to control neurons (Supplemental Figure 8). These results further confirm that TNF-α selectively enhances Nav1.6 currents.

TNF-α mimics the effect of exosomes on primary neurons and is counteracted by Infliximab

To verify whether TNF-α elicits increased firing activity comparable to that observed with U87 and patients' exosomes, hippocampal neurons were treated with different concentrations of TNF-α and spontaneous firing was assessed. As shown in Figure 7, A-F, incubation with 1 ng/ml TNF-α for 24 h induced increased spontaneous firing rate (green trace), which further increased when 10 ng/ml were used (blue trace). Collected data from n=8 and 9 neurons showed that the mean spontaneous firing rate was 0.97+/-0.2 Hz and 2.9+/-0.84 Hz following incubation with 1 and 10 ng/ml TNF-α respectively, while in control neurons values of 0.23±0.15 Hz were observed (Figure 7D). Similar to the incubation with exosomes, the RMP approached the threshold required for spike activation: 1 ng/ml TNF-α depolarized the neurons to -51.5+/-3.4 mV and 10 ng/ml TNF-α to -43.9+/-1.28 mV; these values are significantly different to those of control neurons, which showed a RMP of -71.5+/-3.6 mV (Figure 7E). TNF-α also shifted the activation curve for the inward current to more negative voltages, similarly to patients' exosomes (Supplemental Figure 9). The effect of TNF-α and exosomes, however, was not completely identical. In fact, following incubation with 10 ng/ml

TNF-α, APs showed a more pronounced undershoot of -5 mV±4.6 mV (Supplemental Figure 10A), and voltage clamp experiments showed an activation of a type-A outward current with a higher amplitude in treated cells (Supplemental Figure 10, B and C), suggesting that TNF-α affected also K^+ currents.

To further corroborate our findings, neuronal cultures were pre-incubated with 1.5 ng and 2.5 ng of Infliximab followed by treatment with S479 exosomes (Figure 7, G-M). At the Infliximab lower concentration (orange traces and symbols), neurons showed an average RMP of -43.6±0.51 mV, spike threshold of -31.4±1.36 mV and AP frequency of 1.64±0.27 Hz, values that were not different to those of neurons treated only with exosomes (red traces and symbols) where RMP, AP threshold and activity frequency were -44.2±3.6 mV, -36.42±3.1 mV and 2.26±0.58 Hz, respectively. At the higher concentration, Infliximab abolished the increased excitability induced by exosomes, as evidenced by a RMP of -68.1±3.7 mV, an AP threshold of -40.5±2 mV and an AP frequency of 0.084±0.032 Hz (purple traces and symbols). These values were comparable to those of control neurons (black traces and symbols) with regards to RMP (-58.7±2 mV), spike threshold (-37.4±1 mV) and frequency of spikes (0.13±0.049 Hz). In summary, these results demonstrate that TNF-α is sufficient to trigger hyperexcitability in primary neurons. Therefore, the similar effect seen with exosomes is attributable to the presence of TNF-α.

Discussion

In the present manuscript we propose that exosomes are important players in the origin of BTRE. We identify exosomal TNF-α as a key factor to induce neural hyperexcitability and we propose the use of the FDA approved drug Infliximab, an inhibitor of TNF-α commonly used to treat rheumatoid arthritis (76–78), as a novel agent to treat BTRE.

Epilepsy and brain tumors. In BTRE the causes of epilepsy are diverse and not completely understood. We tested the effect of exosomes derived from 8 patients with glioma and in 7/8 cases exosomes induced heightened firing in hippocampal neurons. This effect was specific to glioma-derived exosomes, as it was not observed with exosomes derived from human astrocytes. Importantly, exosomes derived from GSCs and GASCs give very similar results, suggesting that the mechanism under study is conserved between the two types of glioma cells. However, exosomes derived from different regions within or around the brain tumor have different action: we observed a general trend in the shift of RMP toward more depolarized values, which in one case resulted in a clear increase of neuronal firing frequency and remarkably, this region was also described as the most aggressive by histochemical analysis. Indeed, the different effects observed with the various exosomal pools could also be due to the severity of the tumor (47). In addition, the removal of a section of the tumor resulted in the cessation of epileptic discharges in a nearby region. Altogether, our data further underline the complexity of the cellular mechanisms underlying BTRE. Indeed, some specific brain tumors, such as dysembryoplastic neuroepithelial tumors and gangliogliomas have a high propensity to lead to epilepsy. Cortical tumors in the frontal, temporal and parietal cortex tend to develop more frequent epileptic seizures (4). It has been suggested that permanent epileptic seizures require specific and complex changes in the microenvironment that are not possible in fast growing tumors (79). In our experiments hyperexcitability is unlikely to be caused by an

excessive level of glutamate, as it occurs in different cases of epilepsy, as we did not add any glutamate in any form to our cultures.

Thus, the causes of BTRE are diverse and accordingly, commonly used antiepileptic drugs, such as lamotrigine, lacosamide, pregabalin, topiramate and levetiracetam, are characterized by a wide range of mechanisms of action. Lamotrigine acts primarily as a Nav channels blocker (80), but its spectrum of action is broad. Similarly, Lacosamide targets Nav channels prolonging their inactivation, thereby limiting the maximal rate for AP firing (81). Pregabalin and gabapentinoid primarily inhibit Ca^{2+} channels (82). The molecular mechanisms of the action of topiramate and levetiracetam are less understood but could involve not only effects on Na^{+} and Ca^{2+} channels and neurotransmitter release (83), but also other not yet identified targets (84). According to our data, Nav channel blockage should effectively reduce BTRE and indeed, we show that NBI-921352 / Zandatrigine, a specific blocker of Nav1.6 channels, abolishes the hyperactivity induced by exosomes and hyperpolarizes the RMP. In accordance with this idea, mutations that impair Nav1.6 functionality confer resistance to seizures (85). However, we cannot exclude that the observed effect would impact, besides epilepsy, also on patients' motor/cognitive abilities, depending on the brain area involved (see Fig. 3). The use of more specific inhibitors / blockers could reduce the risk of adverse effects when employed within a clinical therapy.

The content of GBM exosomes and the effect of TNF-α. EVs and exosomes released by U87 cells and brain tumors (13, 86) contain proteins, mRNA, and various kind of microRNAs (87). The most abundant type of proteins present in GBM exosomes are cytokines (86, 88). Cytokines are a big family of proteins comprising interleukins (IL)1–15, growth factors, colony-stimulating factors, interferons (IFN) α, β, and γ, tumor necrosis factor (TNF), and chemokines. TNF-α is one of the most important cytokines acting as a host defense triggering inflammatory responses within the nervous system (89). Its signaling is initiated by TNF-α binding to two receptors, TNFR1 and TNFR2, differentially expressed in cells. TNF-α induces an almost

steady and spontaneous firing in healthy cerebral neurons, in agreement with previous reports (27–29). Incubation with TNF-α leads to Na^+ channels overexpression both in cortical cultures (66) and DRG neurons (90), often with a specific effect on Nav1.6 (29, 66, 91–93). In line with these findings, our results confirm the overexpression of Nav1.6 and Nav1.7 channels in primary hippocampal neurons exposed to U87- and patient-derived exosomes, as well to TNF-α. Concerning the possible underlying mechanisms, since we observe an increase in transcription of selected Nav, inhibiting protein synthesis could indeed partially block the effect of exosomes. However, an increase in membrane targeted channels and/ or changes in the kinetics of their activation / inactivation [due to phosphorylation or other post-translational mechanisms, (94)] could also play a major role. We observed a significant shift of the activation curve towards more negative membrane potentials upon incubation with 10 ng/ml TNF-α (Fig. S5), while in previous reports the shift was not larger than just few mV. In these reports measured currents were in the order of some nA, so that the quality of the space clamp was not as good as when currents selected for the analysis were less than 1 nA. Nav1.6 channels are low-threshold in contrast to Nav1.2 channels, which are high-threshold, and in cerebral neurons Nav1.2 channels are activated at voltages 10-15 mV more depolarized than those for Nav1.6. In DRG neurons, the midpoints of activation are -24.4 and -36 mV for Nav1.2 and $Na_v1.6$, respectively, and the threshold for activation is -57 and -70 mV for Nav1.6 and Nav1.2, respectively (95). Therefore, if TNF-α induces Nav1.6 channels over-expression, patch clamp experiments from cerebral neurons – where Nav1.2 and Nav1.6 are the most expressed Na^+ channels – are expected to cause a shift Na^+ current half-activation towards hyperpolarized values.

Another important issue is the possible heterogeneous effect of Nav1.6 overexpression in different neural subtypes. Our results showed that exosomes and the subsequent activation of TNF-α induce hyperexcitability in both pyramidal and bipolar neurons, consistent with the expression of Nav1.6 in both neural subtypes (96). Additionally, this hyperexcitability is not decreased, but rather often increased, in the presence of large synaptic inputs. The increased

spontaneous activity in pyramidal neurons is largely independent of the GABAergic input, suggesting that bipolar interneurons may be uncoupled from network firing. This could be due to a disproportionate depolarizing effect on these neurons, highlighting a possible mechanism in which the glutamatergic input exceeds the inhibitory input. However, to better understand this mechanism, future work should take into account the variability within inhibitory neurons, which differ in quantity depending on the cortical area. For example, in the primary visual cortex, there are at least 13 distinct GABAergic subtypes (97).

Of note, in the present manuscript we have not addressed the issue whether the overexpression of Nav1.6 occurs preferentially in low or high grade glioma; this important aspect of BRTE will be dealt properly in a manuscript currently in preparation.

In conclusion, we provide evidence suggesting that exosomes released by glioma trigger in some patients neuronal hyperexcitability. This action is likely to be mediated by exosomal TNF-α, which leads to Nav1.6 over-expression. Given the electrical properties of Nav1.6 channels, it is not surprising that their overexpression generates hyperexcitability. We propose that Nav1.6 overexpression is an important factor of BTRE, but certainly not the only cause, as changes of synaptic transmission and an excess of glutamate release also may play a major role. Under our experimental conditions Infliximab, an inhibitor of TNF-α, displayed a clear anti-epileptogenic action. Infliximab does not cross the BBB, however brain penetrating forms of anti-TNFα antibodies could be re-engineered as IgG fusion proteins with a BBB molecular Trojan horse, such as the mAb against the human insulin receptor (HIR)(98). In this case, Infliximab is expected to ameliorate symptoms correlated to neuronal hyperexcitability, such as cognitive and motor deficts, as well as epileptic manifestations.

Methods

Sex as a biological variable. Primary hippocampal neurons were obtained from P2-P3 Wistar rat pups (see below), whose sex was non identified at the time of dissection. Therefore, we did not consider sex as a biological variable in our in vitro experiments on rodent cells.
For what concerns patient-derived cells, our samples derived from 6 males and 2 female patients. Sex was not considered as a biological variable in our in vitro experiments on patient-derived cells.

Cell cultures. Primary hippocampal neuron cultures were performed using Wistar rats (P2-P3). After enzymatic dissociation of hippocampal tissue with a solution containing NaCl 136.9 mM, KCl 4.9 mM, Na_2HPO_4 7 mM, 4-(2-hydroxyethyl)-1-piperazineethanesulfonic acid (HEPES) 25.2 mM, $NaHCO_3$ 4.2 mM, Kinurenic Acid 200 µM and D(-)-2-Amino-5-phosphonopentanoic acid (APV) 25 µM (all from Sigma-Aldrich®), neurons were collected by centrifugation at 100 x g for 5 min and then plated on 15 mm glass coverslips (Menzel-Glaser, #CB00150RA1) previously coated with Poly-L-Ornithine (Sigma-Aldrich®, #P4957) 0.5 µg/ml, and cultured in Neural Basal-A Medium (ThermoFisher Scientific, #21103049) supplemented with GlutaMAX™ Supplement (ThermoFisher Scientific, #35050061), Gentamicin solution 10 mg/mL (Sigma-Aldrich®, #G1272) and B27™ Supplement (ThermoFisher Scientific, #17504044) at 37°C, 5% CO_2 and 95% relative humidity.

Human U87 GBM cells (#89081402, Sigma-Aldrich®) were cultured in DMEM GlutaMAX™ (#31966047 Life Technologies Gibco®) supplemented with 10% fetal bovine serum (#ECS0180L Euroclone) and 1% Penicillin-Streptomycin (#ECB3001D Euroclone). The cultures were maintained at 37°C, 5% CO_2 and 95% relative humidity. Medium was replaced every 3 days and cultures were split at 70-80% confluence.

Human Astrocytes (HAs)(Thermo Fisher Scientific #N7805100) were cultured in Dulbecco's Modified Eagle Medium (DMEM) with GlutaMAX™ supplemented with 10% fetal bovine serum (FBS) (Invitrogen, Life Technologies #31966047 and #ECS0180L), 1%

PenStrep (100 U/ml penicillin and 100 µg/ml streptomycin, Thermo Fisher Scientific, #15070063) and N2 Supplement 100X (Thermo Fisher Scientific, #17502048) at 37°C, 5% CO_2 and medium replaced every 3 days. HA-derived exosomes were used as a control to verify the specificity of the effect of the U87 and patients' exosomes.

To obtain patient glioma cells, human GBM samples were collected by the Neurosurgery Department of the Azienda Ospedaliera Universitaria of Udine. Briefly, tissue samples were mechanically/enzymatically dissociated and single-cell suspensions were cultured as previously described (23).

Exosome isolation and characterization. Exosome isolation and characterization were performed as previously described (26). Briefly, supernatants deriving from U87, HA and glioma cells from patients were subjected to exosome isolation using Total Exosome Isolation reagent (Invitrogen, Life Technologies, #4478359) following the manufacturer's protocol. Isolated exosomes were analyzed using a 405 nm (violet) laser at the NanoSight LM10 (Malvern Panalytical) to verify their size and concentration. Hippocampal neurons were treated using $2.1x10^3$ particles (exosomes) per neuron (15 µg/ml) or 4.2×10^3 particles (30 µg/ml) per neuron for 24 h. For each treatment, 30 µl of PBS containing the desired amount of exosomes were added to 2 ml of culture media. For control treatment, fresh culture medium, which was never in contact with cells, was subjected to the same exosome extraction protocol and the pellet resuspended in PBS. Before electrophysiological recording, the culture medium was removed and replaced by the ringer buffer.

AFM imaging. Atomic Force Microscopy (AFM) images were acquired using an MFP-3D Stand Alone AFM (Asylum Research) in dynamic AC-mode in liquid using commercially available silicon cantilevers (#BL-AC40TS-C2, Olympus Micro Cantilevers, nominal spring constant 0.09 N m−1 and resonant frequency 110kHz).

For sample preparation, we incubated a freshly cleaved muscovite mica sheet (Ruby Muscovite Mica Scratch Free Grade V-1, Nanoandmore GMBH) with 20 µl of Poly-L-Ornithine solution 0.01% (Sigma-Aldrich) for 15 min at room temperature (RT). After gentle washing with Milli-Q water, we added a 15 µl drop of exosomes suspension on the poly-ornithine-coated mica surface at RT for 15-30 min to allow vesicles binding through electrostatic interactions. Then we washed 5 times with PBS and imaged the sample in PBS with the AFM microscope. For each sample, 3-5 images with 5 x 5 µm or 10 x 10 µm of scan size and with a resolution of 1024 × 1024 pixels (pixel size ~ 10 x 10 nm) were acquired. AFM images were analysed with the Gwyddion® software to extract vesicle heights and diameters.

Immunofluorescence staining. Primary hippocampal neurons were plated at a density of $1.0x10^5$ on 15-mm coverslips and treated at DIV 7 as following for 24 h: 1) 10 ng/mL TNF-α; 2) 4.2×10^3 U87 exosomes per cell; 3) 4.2×10^3 patients' exosomes per cell; 4) the previous treatments on samples pre-treated for 2 h with the TNF-α inhibitor Infliximab at a concentration of 2.5 µg/ml. All the samples were compared to the negative control, i.e., the culture medium, which was never in contact with cells, subjected to the same exosome extraction procedure. After treatments, the cells were fixed with 4% PFA for 20 min, washed three times with PBS and incubated with glycine 1 mM for 5 min. Following permeabilization with 0.2% Triton X-100 for 5 min, cells were incubated with 5% bovine serum albumin (BSA) blocking solution at RT for 50 min. Then, coverslips were incubated with the following primary antibodies: rabbit polyclonal anti-Nav1.6/SCN8A (ab65166, abcam®, 1:200) and mouse monoclonal anti-βIII Tubulin (ab78078, abcam®, 1:500). After three washes with PBS-0.01% Tween20, the coverslips were incubated with goat anti-rabbit conjugated to Alexa Flour 594 (A11037, Invitrogen®, 1:600) and goat anti-mouse conjugated to Alexa Fluor 488 (A11029, Invitrogen® 1:600) secondary antibodies for 1 h at RT in a dark and wet chamber. To visualize nuclei, incubation with DAPI 0.5 mg/mL (32670, Merck-Sigma®) in PBS for 15 min at RT was performed. Coverslips were mounted with VECTASHIELD® VibranceTM Antifade Mounting Medium (Vector Laboratories, #H-1700). For image acquisition, an inverted Nikon A1R

confocal microscope (Nikon) was used. For each coverslip at least four fields were analyzed. Z stacks were acquired using the NIS Element Advanced Research Software (Nikon) with 40X/0,95 NA air objective and a spatial resolution of 512 pixels. Image analysis and fluorescence quantification were performed using the ImageJ software (Rasband, W.S., ImageJ). For Nav1.6 quantification, only the soma and the neurite initial segments have been considered. The Simple Neurite Tracer ImageJ plugin was applied to βIII tubulin green channel to select the region of interest (ROI) for each neuron. Fluorescence intensity was measured by integrated density (IntDen) and expressed as Corrected Total Cell Fluorescence (CTCF) corresponding to the IntDen minus the product of the area of the cell and the average of mean gray value from three background ROIs.

Quantitative real-time PCR. qRT-PCR was employed to evaluate the Nav1.1, Nav1.2, Nav1.3, Nav1.6 and Nav1.7 Na^+ channels expression. The RNeasy Mini Kit® (QIAGEN, #74104) was used for isolation of total RNA from rat hippocampal neurons treated as previously described for immunofluorescence staining. After RNA extraction, TURBO DNA-freeTM Kit® (Sigma-Aldrich®, #AM1907) was used to remove traces of genomic DNA. Then, cDNA synthesis was performed by Maxima® First Strand cDNA Synthesis Kit (Thermo Scientific, #K1641) and used for quantitative real-time PCR using SYBR Green Supermix (Bio-Rad, #1725270) on a CFX Connect Real-Time PCR Detection System (CFX Maestro Software). Expression levels were normalised to Gapdh and fold change was determined by applying the $2^{-\Delta\Delta Ct}$ method. The following primers were used:

Nav1.1; Scn1ar_fw 5'-AGAAACCCTTGAGCCCGAAG-3',

Scn1ar_rev 5'-CACACTGATTTGACAGCACTTGAA-3'

Nav1.2; Scn2ar_fw 5'-AGGAACGCAAGGACGAAG-3',

Scn 2ar_rev 5'-TCTAATGGGGTTGAAGGGAG-3'

Nav1.3; Scn3ar_fw 5'-CGATGCAATTCACCCTGGAAG-3',

Scn3ar_rev 5'-GTGGCGACGCTGAAGTTCTC-3

Nav1.6 Scn8ar_fw 5'-ATGGTGAGCGGAGATCGAA-3',

Scn8ar_rev 5'-GTGGTCGTGATAGGCTCGTA-3'

Nav1.7 Scn9ar_fw 5'-TCCTTTATTCATAATCCCAGCCTCAC-3',

Scn9ar_rev 5'-GATCGGTTCCGTCTCTCTTTGC-3'

Gapdh, fw 5'-ATCTTCTTGTGCAGTGCCAGCCTCGTC -3'

rev 5'-GAACATGTAGACCATGTAGTTGAGGTCAATGAAGG -3'

Western blotting. After isolation from cell culture medium, exosomes were resuspended in CHAPS Cell Extract Buffer (Cell Signaling Technology, #9852S) supplemented with protease inhibitor cocktail (Thermo Fisher Scientific, # 78430) and 4X Laemmli buffer was added to the samples. Following denaturation at 95°C for 5 min, 30 µg/lane were loaded on 10% SDS-polyacrylamide gel. Proteins were transferred onto Hybond® ECL™ nitrocellulose membrane (Amersham Biosciences, # LC2000) using the semi-dry system Trans-Blot® Turbo™ Transfer System (Biorad, #1704150) set to 1.3 A and 25 V for 1 h. Membrane was blocked in 3% BSA (Sigma-Aldrich®) for 1 h at RT, and then incubated with the primary antibodies rabbit polyclonal to TNF-α (Abcam, ab6671, 1:500) overnight (ON) at 4°C with gentle shaking. Next, three 5 min washes in TBS with 0.1%Tween 20 (Sigma-Aldrich®, # P9416) were performed, and goat anti-rabbit HRP conjugated secondary antibodies (Agilent, #P0449, 1:2000) were added for 1 h at RT. After washing, the membrane was incubated for 3-5 min with Immobilon® ECL Ultra Western HRP Substrate (Sigma-Aldrich®, # 42029053) and images acquired with the transilluminator NineAlliance™ (Uvitec).

TNF-α quantification. Exosomes derived from U87 and patients were lysed in RIPA cell-lysis buffer (NaCl 150mM, Tris-HCl 50mM, nonidet P40 1%, sodium deoxycholate 0.5%, ddH_2O) containing Protease Inhibitor Cocktail 50X (Thermo Scientific™ #78430). Protein concentration was determined with the Pierce™ BCA Protein Assay Kit (Thermo Fisher Scientific™ #23225) and TNF-α content was quantified using ELISA (Enzyme-linked immunosorbent assay) (Cloud-Clone Corp®, #SEA133Hu), as per standard protocol. The

amount of TNF-α per 100 µg of total proteins was determined recording absorbance at 450 nm.

Electrophysiology. Hippocampal neurons (8-12DIV) on coverslips were viewed on a inverted microscope (Olympus IX70), and neuron identification was made by morphology and later during the records in whole cell. Patch electrodes had a 2-5 MΩ resistance and were pulled from borosilicate capillaries (WPI) with a PC-10 puller (Narishige), electrodes containing a intracellular solution of (in mM): 145 KCl, 4 $MgCl_2$, 1 EGTA, 2 Na_2-ATP and 10 HEPES, adjusted to pH 7.2 with KOH. In some experiments to isolate Na^+ current, there was a partial replacement of KCl by 135 mM of CsCl + NaCl 5 mM. Electrophysiological recordings were made using a MultiClamp 700B amplifier controlled by Clampex 10.6 via a Digidata 1550B (Molecular Devices), the sample frequency used to acquire data was 10 kHz and low-pass filtered at 2 kHz.

For current clamp spontaneous activity records, neurons were held at I=0 for 3 or 5 min before of a gap free registration for additional 4 min. Then on the same cell synaptic spontaneous currents (4 min, -70 mV) and the activation of voltage gated currents by step-depolarization from a holding potential of -70 mV were recorded in voltage clamp configuration. To check if cells that did not show spontaneous activity were neurons, a slow hyperpolarizing current was applied until -70 mV, then a step-depolarization protocol was performed by injecting a current by 1.5 s with increasing amplitude of 50 pA in each step until triggering action potentials. Before current injection, bridge balance and pipette capacitance neutralization were carefully monitored and adjusted throughout experiments by application of low frequency (50 Hz), low amplitude (10-40 pA) current steps. AP properties were obtained from the mean phase plot (dV/dt) of 10 AP randomly chosen during the record. Statistical analysis of spike frequency, maximum currents, IV curves, and conductance plots were made by IGOR pro.

The extracellular ringer contained (in mM): 140 NaCl, 5 KCl, 2 $CaCl_2$, 1 $MgCl_2$, 10 HEPES, and 10 glucose, pH 7.4. In some experiments to check the ionic permeability to Na^+, two types

of solution were used: the first one had 70 mM of NaCl + 70 mM of NMDG-Cl to decrease the amplitude of Na^+ currents, then all the other components were the same than the extracellular ringer plus a blocker of Ca^{2+} gated conductance ($CdCl_2$ 100 μM), the second was prepared with $CdCl_2$ and isosmolar replacement of NaCl by NMDG-Cl. To change solutions, the set up was equipped with an eight-in-one multibarrel perfusion pencil connected to a ValveLink8.2 pinch valve perfusion system (Automate Scientific). All compounds and chemicals were obtained from Sigma-Aldrich, unless otherwise stated. All liquid junction potentials (LJP) for the solutions used were calculated using the pClampex software (Axon Instruments), obtaining values between 1.2 to 3.8 mV.

Surgical procedures on glioma patients. The surgical procedures were performed using cortical and subcortical mapping methods in accordance with the usual surgical technique (99, 100). In addition to direct electrical stimulation (DES), a performance-based resection related to real-time neuropsychological testing (RTNT) was performed in those cases selected for awake surgery (101). Intraoperative neurophysiological monitoring and intraoperative ECoG were performed in all cases as previously described (Axon System Eclipse®)(102).

Statistical analysis. Results are presented as mean±SD or mean±SEM, as indicated in figure legends. Statistical analysis was performed through GraphPad (GraphPad Prism 7, GraphPad soft-ware, San Diego, CA, USA). The two-tailed unpaired Student's t-test was used to compare two normally distributed sample groups, and equality of variances was tested through the F test; when more than two groups were compared, one-way ANOVA followed by Bonferroni's post-hoc multiple comparison tests was performed, and equality of variances tested through the Brown–Forsythe's and Bartlett's test. The Wilcoxon–Mann–Whitney U test and Kruskal–Wallis test were used to compare two or more non-normally distributed sample groups, respectively. A p-value < 0.05 was considered significant. No predictive statistical methods were used to predetermine sample sizes; however, we adopted sample sizes

(indicated in figure legends) in the same range as those previously reported in the literature for similar experiments. The ROUT method with Q=1% was used to identify outliers. No randomization method was followed to allocate samples to the various experimental groups. Investigators were blinded to group allocation and when assessing the outcome of the experiments.

Study approval. The use of primary neurons was approved by the Local Veterinary Service, by the SISSA Ethics Committee board and by the National Ministry of Health. All the procedures were conducted according to the guidelines of the Italian Animal Welfare Act and to the European Union guidelines for animal care (d.1.116/92; 86/609/C.E.).
The protocol for human samples was approved by the local Ethics Committee, Comitato Etico Unico Regionale del Friuli Venezia Giulia (protocol number 718345, opinion 196/2014/Em).

Data Availability: The data that support the findings of this study are available from the corresponding author upon reasonable request. The ‘Supporting data values’ file is provided as supplementary material.

Author contributions

C.A.S.T. performed and analyzed electrophysiological experiments, discussed the results and contributed to paper writing; R.S. performed and analyzed biochemical and immunocytochemical experiments, discussed the results and contributed to paper writing; F.S. and C.D'A. performed and analyzed biochemical and immunocytochemical experiments; I.M., I.G.R., T.I. and D.C. derived and cultured GSCs and GASCs, discussed the results and contributed to paper writing; P.P. characterized the biophysical properties of exosomes; A.M. supervised electrophysiological experiments and financially supported the project; M.S. performed neurosurgery and contributed to paper writing; F.C. supervised the biochemical and immunocytochemical experiments and wrote the paper; V.T. designed the project, supervised all the experiments, discussed the results, wrote the paper and financially supported the project. C.A.S.T. and R.S. are co-first authors. Because of the prevalence of electrophysiological data, C.A.S.T. is assigned the first name.

Acknowledgements

This work has received financial support from: Friuli Venezia-Giulia (FVG) project "Progetto di ricerca traslazionale e sviluppo preclinico di strategie terapeutiche innovative e predittive per l'ottimizzazione del trattamento di tumori cerebrali" to V.T.; FVG project "ARES" to V.T.; FVG project "Glioblastoma" to V.T. We are grateful to M. Pusch for critical discussion and advice and the SISSA technical staff for their assistance.

Declaration of Interest Statement

The authors declare that they do not have any competing financial interests in relation to the work described.

References

1. Brogna C, et al. Brain tumors and epilepsy. *Expert Rev Neurother*. 2008;8(6):941–955.

2. Englot DJ, et al. Epilepsy and brain tumors. *Handb Clin Neurol*. 2016;134:267–285.

3. Saeedi S, et al. The emerging role of exosomes in mental disorders. *Transl Psychiatry*. 2019;9(1):122.

4. Adhikari S, et al. Pathogenesis and Management of Brain Tumor-Related Epilepsy. In: Debinski W, ed. *Gliomas*. Brisbane (AU): Exon Publications; 2021.

5. Ius T, et al. Predictors of postoperative seizure outcome in low grade glioma: from volumetric analysis to molecular stratification. *Cancers (Basel)*. 2020;12(2). https://doi.org/10.3390/cancers12020397.

6. Whitehead CA, et al. Extracellular vesicles and their role in glioblastoma. *Crit Rev Clin Lab Sci*. 2019;1–26.

7. Yekula A, et al. Extracellular vesicles in glioblastoma tumor microenvironment. *Front Immunol*. 2019;10:3137.

8. Rajendran L, et al. Emerging roles of extracellular vesicles in the nervous system. *J Neurosci*. 2014;34(46):15482–15489.

9. Nieland L, et al. Extracellular Vesicle-Mediated Bilateral Communication between Glioblastoma and Astrocytes. *Trends Neurosci*. 2021;44(3):215–226.

10. Sun Z, et al. Glioblastoma Stem Cell-Derived Exosomes Enhance Stemness and Tumorigenicity of Glioma Cells by Transferring Notch1 Protein. *Cell Mol Neurobiol*. 2020;40(5):767–784.

11. Skog J, et al. Glioblastoma microvesicles transport RNA and proteins that promote tumour growth and provide diagnostic biomarkers. *Nat Cell Biol*. 2008;10(12):1470–1476.

12. Akers JC, et al. miRNA contents of cerebrospinal fluid extracellular vesicles in glioblastoma patients. *J Neurooncol*. 2015;123(2):205–216.

13. Gao X, et al. Gliomas Interact with Non-glioma Brain Cells via Extracellular Vesicles. *Cell Rep*. 2020;30(8):2489-2500.e5.

14. Couch Y, et al. A brief history of nearly EV-erything - The rise and rise of extracellular vesicles. *J Extracell Vesicles*. 2021;10(14):e12144.

15. Xiao L, et al. Function of exosomes in neurological disorders and brain tumors. *Extracell Vesicles Circ Nucl Acids*. 2021;2:55–79.

16. Lathia JD, et al. Cancer stem cells in glioblastoma. *Genes Dev*. 2015;29(12):1203–1217.

17. Gimple RC, et al. Glioblastoma stem cells: lessons from the tumor hierarchy in a lethal cancer. *Genes Dev*. 2019;33(11–12):591–609.

18. Lah TT, et al. Brain malignancies: Glioblastoma and brain metastases. *Semin Cancer Biol*. 2020;60:262–273.

19. Bhat KPL, et al. Mesenchymal differentiation mediated by NF-κB promotes radiation resistance in glioblastoma. *Cancer Cell*. 2013;24(3):331–346.

20. Jeon H-M, et al. Inhibitor of differentiation 4 drives brain tumor-initiating cell genesis through cyclin E and notch signaling. *Genes Dev*. 2008;22(15):2028–2033.

21. Rheinbay E, et al. An aberrant transcription factor network essential for Wnt signaling and stem cell maintenance in glioblastoma. *Cell Rep*. 2013;3(5):1567–1579.

22. Théry C, et al. Minimal information for studies of extracellular vesicles 2018 (MISEV2018): a position statement of the International Society for Extracellular Vesicles and update of the MISEV2014 guidelines. *J Extracell Vesicles*. 2018;7(1):1535750.

23. Bourkoula E, et al. Glioma-associated stem cells: a novel class of tumor-supporting cells able to predict prognosis of human low-grade gliomas. *Stem Cells*. 2014;32(5):1239–1253.

24. Clavreul A, et al. Identification of two glioblastoma-associated stromal cell subtypes with different carcinogenic properties in histologically normal surgical margins. *J Neurooncol*. 2015;122(1):1–10.

25. Manini I, et al. Semaphorin-7A on Exosomes: A Promigratory Signal in the Glioma Microenvironment. *Cancers (Basel)*. 2019;11(6). https://doi.org/10.3390/cancers11060758.

26. Spelat R, et al. The dual action of glioma-derived exosomes on neuronal activity: synchronization and disruption of synchrony. *Cell Death Dis*. 2022;13(8):705.

27. Park KM, Bowers WJ. Tumor necrosis factor-alpha mediated signaling in neuronal homeostasis and dysfunction. *Cell Signal*. 2010;22(7):977–983.

28. Leo M, et al. Modulation of Voltage-Gated Sodium Channels by Activation of Tumor Necrosis Factor Receptor-1 and Receptor-2 in Small DRG Neurons of Rats. *Mediators Inflamm*. 2015;2015:124942.

29. Ding H-H, et al. TNF-α/STAT3 pathway epigenetically upregulates Nav1.6 expression in DRG and contributes to neuropathic pain induced by L5-VRT. *J Neuroinflammation*. 2019;16(1):29.

30. Lee C, et al. Glycosylation profile and biological activity of Remicade® compared with Flixabi® and Remsima®. *MAbs*. 2017;9(6):968–977.

31. Andolfi L, et al. Investigation of adhesion and mechanical properties of human glioma cells by single cell force spectroscopy and atomic force microscopy. *PLoS ONE*. 2014;9(11):e112582.

32. Parisse P, et al. Atomic force microscopy analysis of extracellular vesicles. *Eur Biophys J*. 2017;46(8):813–820.

33. Perissinotto F, et al. Multi-technique analysis of extracellular vesicles: not only size matters. Elsevier; 2020:157–177.

34. Genc S, et al. Potential Neurotoxic Effects of Glioblastoma-Derived Exosomes in Primary Cultures of Cerebellar Neurons via Oxidant Stress and Glutathione Depletion. *Antioxidants (Basel)*. 2022;11(7). https://doi.org/10.3390/antiox11071225.

35. Pinet S, et al. TrkB-containing exosomes promote the transfer of glioblastoma aggressiveness to YKL-40-inactivated glioblastoma cells. *Oncotarget*. 2016;7(31):50349–50364.

36. Sun X, et al. Glioma stem cells-derived exosomes promote the angiogenic ability of endothelial cells through miR-21/VEGF signal. *Oncotarget*. 2017;8(22):36137–36148.

37. Marton S, et al. SOD1G93A Astrocyte-Derived Extracellular Vesicles Induce Motor Neuron Death by a miRNA-155-5p-Mediated Mechanism. *ASN Neuro*. 2023;15:17590914231197528.

38. Kandel ER, et al. Transient and long-lasting electrical responses to direct hippocampal stimulation. *Am J Physiol*. 1960;198:687–692.

39. Malik R, et al. Mapping the electrophysiological and morphological properties of CA1 pyramidal neurons along the longitudinal hippocampal axis. *Hippocampus*. 2016;26(3):341–361.

40. Prestigio C, et al. Spike-Related Electrophysiological Identification of Cultured Hippocampal Excitatory and Inhibitory Neurons. *Mol Neurobiol*. 2019;56(9):6276–6292.

41. Hille B. *Ion Channels of Excitable Membranes*. Sunderland, Mass: Sinauer Associates is an imprint of Oxford University Press; 2001.

42. Colin-Le Brun I, et al. Spontaneous synaptic activity is required for the formation of functional GABAergic synapses in the developing rat hippocampus. *J Physiol (Lond)*. 2004;559(Pt 1):129–139.

43. Draguhn A, et al. A simple hardware model for the direct observation of voltage-clamp performance under realistic conditions. *J Neurosci Methods*. 1997;78(1–2):105–113.

44. Rauti R, et al. Graphene oxide flakes tune excitatory neurotransmission in vivo by targeting hippocampal synapses. *Nano Lett*. 2019;19(5):2858–2870.

45. Clark GD, et al. Enhancement of hippocampal excitatory synaptic transmission by platelet-activating factor. *Neuron*. 1992;9(6):1211–1216.

46. Markram H, et al. Reconstruction and simulation of neocortical microcircuitry. *Cell*. 2015;163(2):456–492.

47. Manini I, et al. Heterogeneity Matters: Different Regions of Glioblastoma Are Characterized by Distinctive Tumor-Supporting Pathways. *Cancers (Basel)*. 2020;12(10). https://doi.org/10.3390/cancers12102960.

48. Buchhalter JR, Dichter MA. Electrophysiological comparison of pyramidal and stellate nonpyramidal neurons in dissociated cell culture of rat hippocampus. *Brain Res Bull*. 1991;26(3):333–338.

49. Wang D, et al. Fluorescein-based chromo-fluorescent probe for zinc in aqueous solution: Spirolactam ring opened or closed? *Sensors and Actuators B: Chemical*. 2014;201:246–254.

50. Tomassoni-Ardori F, et al. Generation of functional mouse hippocampal neurons. *Bio Protoc*. 2020;10(15). https://doi.org/10.21769/bioprotoc.3702.

51. Kaech S, Banker G. Culturing hippocampal neurons. *Nat Protoc*. 2006;1(5):2406–2415.

52. Dotti CG, et al. The establishment of polarity by hippocampal neurons in culture. *J Neurosci*. 1988;8(4):1454–1468.

53. Gu Y, et al. Effects of lead on voltage-gated sodium channels in rat hippocampal CA1 neurons. *Neuroscience*. 2005;133(3):679–690.

54. Apps DK. Ionic channels of excitable membranes (second edition). *FEBS Lett*. 1992;306(2–3):277–278.

55. Guo F, et al. The up-regulation of voltage-gated sodium channels subtypes coincides with an increased sodium current in hippocampal neuronal culture model. *Neurochem Int*. 2013;62(3):287–295.

56. Remy C, et al. Modulation of voltage-dependent sodium channels by the delta-agonist SNC80 in acutely isolated rat hippocampal neurons. *Neuropharmacology*. 2004;47(7):1102–1112.

57. Wengert ER, Patel MK. The role of the persistent sodium current in epilepsy. *Epilepsy Curr*. 2021;21(1):40–47.

58. Deng P-Y, Klyachko VA. Increased persistent sodium current causes neuronal hyperexcitability in the entorhinal cortex of fmr1 knockout mice. *Cell Rep*. 2016;16(12):3157–3166.

59. Kiss T. Persistent Na-channels: origin and function. A review. *Acta Biol Hung*. 2008;59 Suppl:1–12.

60. Chen J, et al. Tumor-derived extracellular vesicles: Regulators of tumor microenvironment and the enlightenment in tumor therapy. *Pharmacol Res*. 2020;159:105041.

61. Caponnetto F, et al. The miRNA Content of Exosomes Released from the Glioma Microenvironment Can Affect Malignant Progression. *Biomedicines*. 2020;8(12). https://doi.org/10.3390/biomedicines8120564.

62. Munich S, et al. Dendritic cell exosomes directly kill tumor cells and activate natural killer cells via TNF superfamily ligands. *Oncoimmunology*. 2012;1(7):1074–1083.

63. Gao W, et al. Exosomes derived from mature dendritic cells increase endothelial inflammation and atherosclerosis via membrane TNF-α mediated NF-κB pathway. *J Cell Mol Med*. 2016;20(12):2318–2327.

64. Li X, et al. Interleukin-6 inhibits voltage-gated sodium channel activity of cultured rat spinal cord neurons. *Acta Neuropsychiatr*. 2014;26(3):170–177.

65. Zhou C, et al. Interleukin-1β inhibits voltage-gated sodium currents in a time- and dose-dependent manner in cortical neurons. *Neurochem Res*. 2011;36(6):1116–1123.

66. Chen W, et al. Tumor necrosis factor-α enhances voltage-gated Na^+ currents in primary culture of mouse cortical neurons. *J Neuroinflammation*. 2015;12:126.

67. de Macedo FHP, et al. TNF-α mediated upregulation of NaV1.7 currents in rat dorsal root ganglion neurons is independent of CRMP2 SUMOylation. *Mol Brain*. 2019;12(1):117.

68. Pathare G, et al. Acute regulated expression of pendrin in human urinary exosomes. *Pflugers Arch*. 2018;470(2):427–438.

69. Kugeratski FG, et al. Quantitative proteomics identifies the core proteome of exosomes with syntenin-1 as the highest abundant protein and a putative universal biomarker. *Nat Cell Biol*. 2021;23(6):631–641.

70. Hu W, et al. Distinct contributions of Na(v)1.6 and Na(v)1.2 in action potential initiation and backpropagation. *Nat Neurosci*. 2009;12(8):996–1002.

71. Goldin AL. Resurgence of sodium channel research. *Annu Rev Physiol*. 2001;63:871–894.

72. Rabert DK, et al. A tetrodotoxin-resistant voltage-gated sodium channel from human dorsal root ganglia, hPN3/SCN10A. *Pain*. 1998;78(2):107–114.

73. Sakkaki S, et al. Focal dorsal hippocampal nav1.1 knock down alters place cell temporal coordination and spatial behavior. *Cereb Cortex*. 2020;30(9):5049–5066.

74. Estacion M, et al. A sodium channel mutation linked to epilepsy increases ramp and persistent current of Nav1.3 and induces hyperexcitability in hippocampal neurons. *Exp Neurol*. 2010;224(2):362–368.

75. Johnson JP, et al. NBI-921352, a first-in-class, NaV1.6 selective, sodium channel inhibitor that prevents seizures in Scn8a gain-of-function mice, and wild-type mice and rats. *eLife*. 2022;11. https://doi.org/10.7554/eLife.72468.

76. Zhang H, et al. Therapeutic potential of TNFα inhibitors in chronic inflammatory disorders: Past and future. *Genes Dis*. 2021;8(1):38–47.

77. Iannone F, et al. Subcutaneously-Administered Infliximab in the Management of Rheumatoid Arthritis: A Short Narrative Review of Current Clinical Evidence. *J Inflamm Res*. 2022;15:3259–3267.

78. Liu Y, et al. Fine Comparison of the Efficacy and Safety Between GB242 and Infliximab in Patients with Rheumatoid Arthritis: A Phase III Study. *Rheumatol Ther*. 2022;9(1):175–189.

79. Chen DY, et al. Tumor-related epilepsy: epidemiology, pathogenesis and management. *J Neurooncol*. 2018;139(1):13–21.

80. Larry Jameson J, et al. *Harrison's Principles of Internal Medicine, Twentieth Edition (Vol.1 & Vol.2)*. New York: McGraw-Hill Education / Medical; 2018.

81. Doty P, et al. Development of lacosamide for the treatment of partial-onset seizures. *Ann N Y Acad Sci*. 2013;1291:56–68.

82. Frampton JE. Pregabalin: a review of its use in adults with generalized anxiety disorder. *CNS Drugs*. 2014;28(9):835–854.

83. Linde M, et al. Topiramate for the prophylaxis of episodic migraine in adults. *Cochrane Database Syst Rev*. 2013;2013(6):CD010610.

84. Cavanna AE. *Behavioural Neurology of Anti-epileptic Drugs*. Oxford University Press; 2018.

85. Makinson CD, et al. Role of the hippocampus in Nav1.6 (Scn8a) mediated seizure resistance. *Neurobiol Dis*. 2014;68:16–25.

86. Sharma KD, et al. Glioma-derived exosomes drive the differentiation of neural stem cells to astrocytes. *PLoS ONE*. 2020;15(7):e0234614.

87. de Mooij T, et al. Short non-coding RNA sequencing of glioblastoma extracellular vesicles. *J Neurooncol*. 2020;146(2):253–263.

88. Iwami K, et al. Cytokine networks in glioma. *Neurosurg Rev*. 2011;34(3):253–63; discussion 263.

89. Mukhara D, et al. Neuroinflammation. *Handb Clin Neurol*. 2020;175:235–259.

90. Chen X, et al. TNF-α enhances the currents of voltage gated sodium channels in uninjured dorsal root ganglion neurons following motor nerve injury. *Exp Neurol*. 2011;227(2):279–286.

91. Zhang X-L, et al. Palmitoylation of δ-catenin promotes kinesin-mediated membrane trafficking of Nav1.6 in sensory neurons to promote neuropathic pain. *Sci Signal*. 2018;11(523). https://doi.org/10.1126/scisignal.aar4394.

92. Ai Y, et al. Role of the voltage-gated sodium channel Nav1.6 in glioma and candidate drugs screening. *Int J Mol Med*. 2023;51(6). https://doi.org/10.3892/ijmm.2023.5249.

93. Cheng S, et al. Soluble tumor necrosis factor-alpha-induced hyperexcitability contributes to retinal ganglion cell apoptosis by enhancing Nav1.6 in experimental glaucoma. *J Neuroinflammation*. 2021;18(1):182.

94. Zybura AS, et al. CaMKII enhances voltage-gated sodium channel Nav1.6 activity and neuronal excitability. *J Biol Chem*. 2020;295(33):11845–11865.

95. Rush AM, et al. Electrophysiological properties of two axonal sodium channels, Nav1.2 and Nav1.6, expressed in mouse spinal sensory neurones. *J Physiol (Lond)*. 2005;564(Pt 3):803–815.

96. Patel RR, et al. Human Nav1.6 Channels Generate Larger Resurgent Currents than Human Nav1.1 Channels, but the Navβ4 Peptide Does Not Protect Either Isoform from Use-Dependent Reduction. *PLoS ONE*. 2015;10(7):e0133485.

97. Tremblay R, et al. Gabaergic interneurons in the neocortex: from cellular properties to circuits. *Neuron*. 2016;91(2):260–292.

98. Pardridge WM. Biologic TNFα-inhibitors that cross the human blood-brain barrier. *Bioeng Bugs*. 2010;1(4):231–234.

99. Ius T, et al. Low-grade glioma surgery in eloquent areas: volumetric analysis of extent of resection and its impact on overall survival. A single-institution experience in 190 patients: clinical article. *J Neurosurg*. 2012;117(6):1039–1052.

100. Ius T, et al. Multimodal integrated approaches in low grade glioma surgery. *Sci Rep*. 2021;11(1):9964.

101. Skrap M, et al. Brain mapping: a novel intraoperative neuropsychological approach. *J Neurosurg*. 2016;125(4):877–887.

102. Lettieri C, et al. Risk factors for intraoperative seizures in glioma surgery: electrocorticography matters. *J Clin Neurophysiol*. [published online ahead of print: April 30, 2021]. https://doi.org/10.1097/WNP.0000000000000854.

Figures and Figure Legends

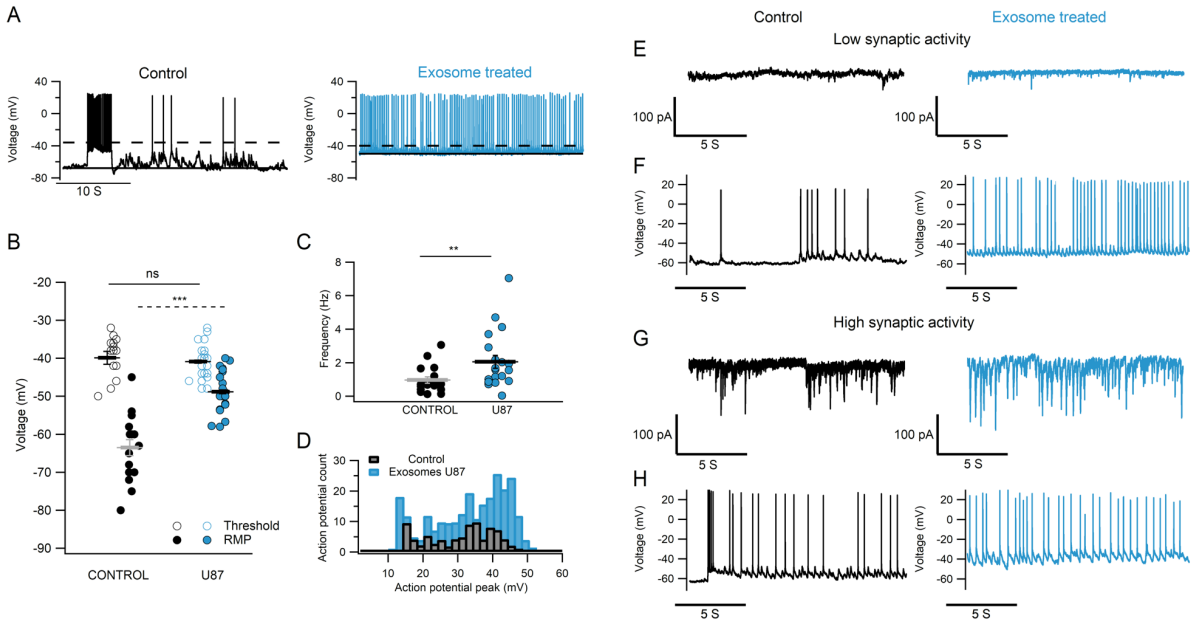

Figure 1: U87 exosomes induce increased spontaneous firing that is independent of the synaptic input. A. Intracellular recordings in current clamp (I=0) from a control hippocampal neuron (left, black trace) and a neuron incubated for 24 h with U87 exosomes (right, blue trace). **B.** Comparison of resting membrane potential (RMP; filled circles) and AP threshold (empty circles). **C.** Spontaneous AP frequency for both conditions. For B and C: n=16 control; n=20-22 treated neurons. ***p<0.001, Mann-Whitney U-test. **D.** AP distribution from 8 randomly selected neurons in control and treated groups. **E.** Neurons exhibiting low synaptic inputs: representative examples of voltage clamp recordings at -70 mV under control and treated conditions to obtain recordings of synaptic currents not contaminated by voltage gated conductances. **F.** Corresponding current clamp recordings from the cells in E, showing increased firing induced by U87 exosomes (blue) **G**. Voltage clamp at -70 mV and **H.** current clamp obtained from a control and U87-treated neuron exhibiting high synaptic inputs.

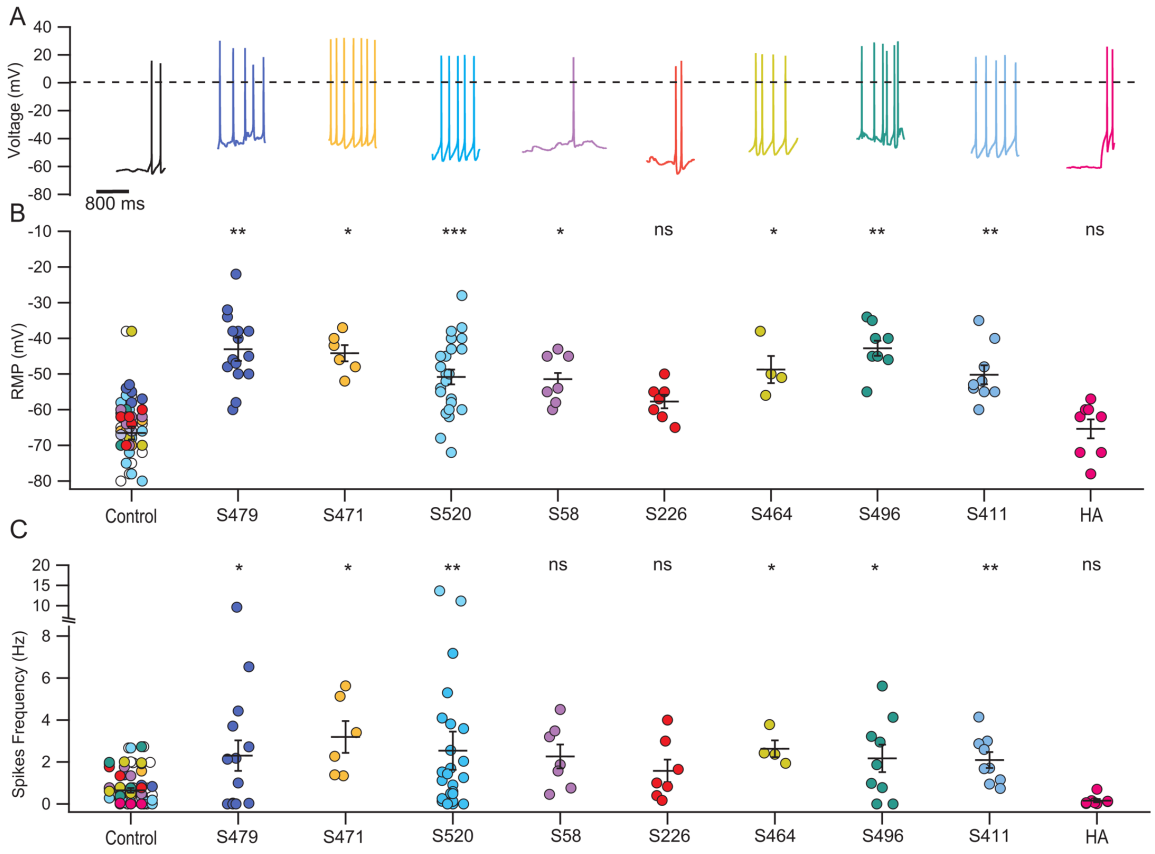

Figure 2: The increase of spontaneous firing is induced also by patient-derived exosomes. A. Representative current clamp recordings from control hippocampal neurons (leftmost black trace), neurons incubated with patients' exosomes (colored traces), and with exosomes obtained from healthy human astrocytes (HA, rightmost pink trace); the dashed black line shows 0 mV. Patients' identification numbers are indicated. **B**. Resting membrane potential (RMP) for all the experimental groups. Values for exosomes derived from patients with an epileptic report are: GASC-S479=-43±2.6 mV and GSC-S496=-42.8±2.13, which are statistically different from the values of their control groups, i.e., -61.7±4.4 mV and -76.8±7.3 mV, respectively. **C**. Spontaneous firing frequency of the same experimental groups. GASC-S479=2.3±0.73 Hz, GSC-S496=2.17±0.65 Hz, the respective controls were 0.56±0.14 Hz and 1.46±0.54 Hz. Data from control neurons for all the experimental groups are over imposed in the leftmost column. Mann-Whitney U test, $p<0.001$ ***; $p<0.01$**, $p<0.05$*, n = 4 to 25.

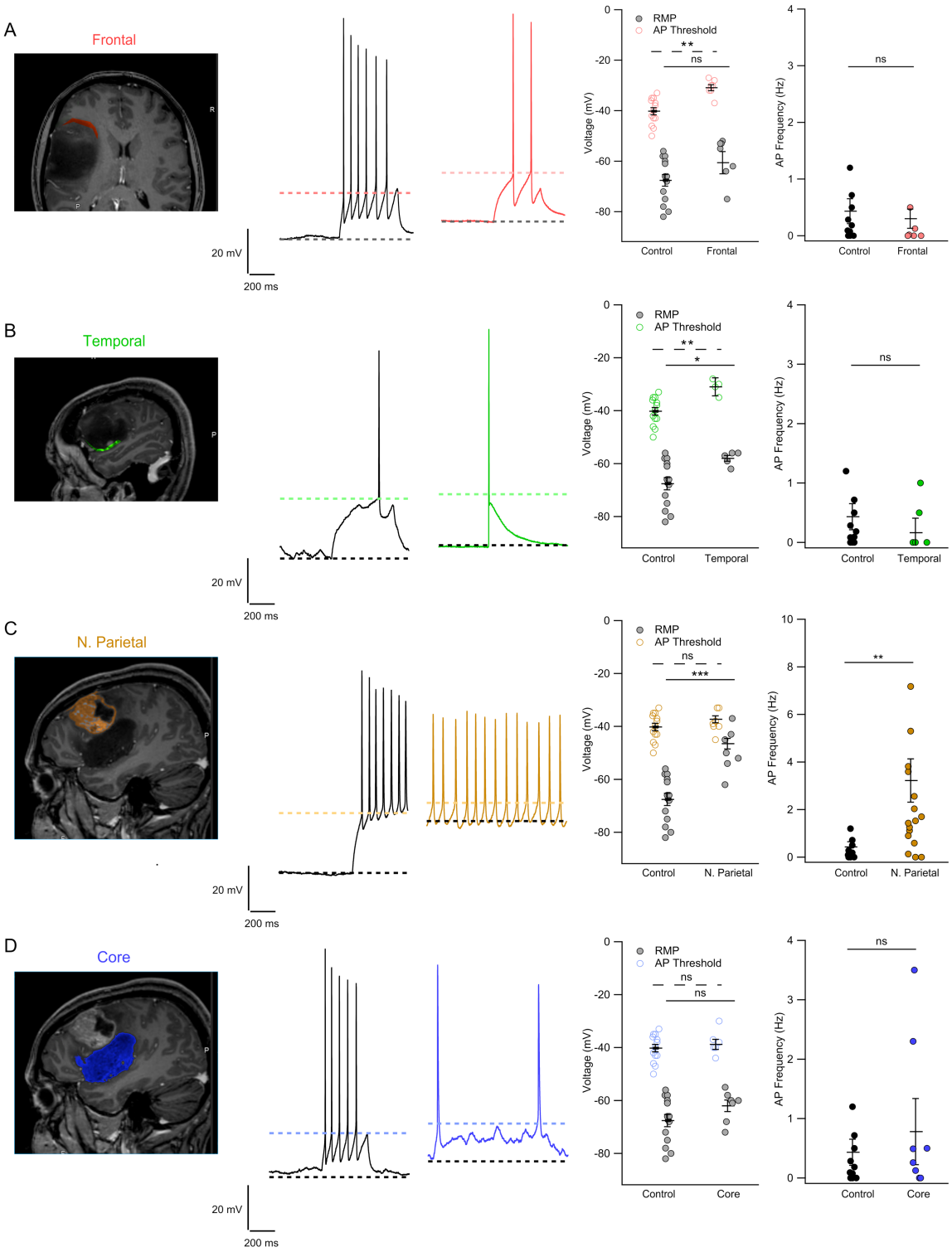

Figure 3: The effect of patient exosomes depends on the region they derived from. Panels show, from left to right: tomography images of the #S520 patient highlighting the different portions of the tumor; traces from control neurons (black) and from neurons treated with exosomes derived from the different tumor areas (colored traces); quantification of RMP,

action potential threshold and AP frequency. **A.** Coronal tomography section showing the tumoral region in close contact to the fronto-parietal lobe highlighted in red. RMP: -67.57±3.31 mV (ctrl) and -59.1±3.2 mV (exosomes); action potential threshold: -40±1.4 mV (ctrl) and -30.8±1.24 mV (exosomes); spike frequency: 0.43±0.22 mV (control) and 0.09±0.07 Hz (exosomes). **B.** Sagittal tomography section showing the temporal border of the tumor highlighted in green. RMP: -58 mV±1.14 mV; action potential threshold: -31±1.5 mV; spike frequency: 0.3±0.2 Hz. Control values as in (A). **C.** Sagittal tomography section showing a tumor nodule localized in the parietal lobe highlighted in yellow. RMP: -46.5 mV±1.95 mV; action potential threshold: -37.3±1.26 mV; spike frequency; 3.22±0.9 Hz. Control values as in (A). **D.** Sagittal tomography section showing the tumor mass localized in the temporal lobe highlighted in blue; exosomes were extracted from the core of this mass. RMP: -62 mV±2.23 mV; action potential threshold: -38.2±2 mV; spikes frequency: 0.9±0.45 Hz. Control values as in (A). Kruskal-Wallis followed by Bonferroni corrected Dunn's test for all groups vs control. *** $p<0.001$, ** $p<0.01$, * $p<0.05$; control n=14 (common to all experimental samples), temporal n=4-5; frontal n=7, parietal n=18, core n=6-8.

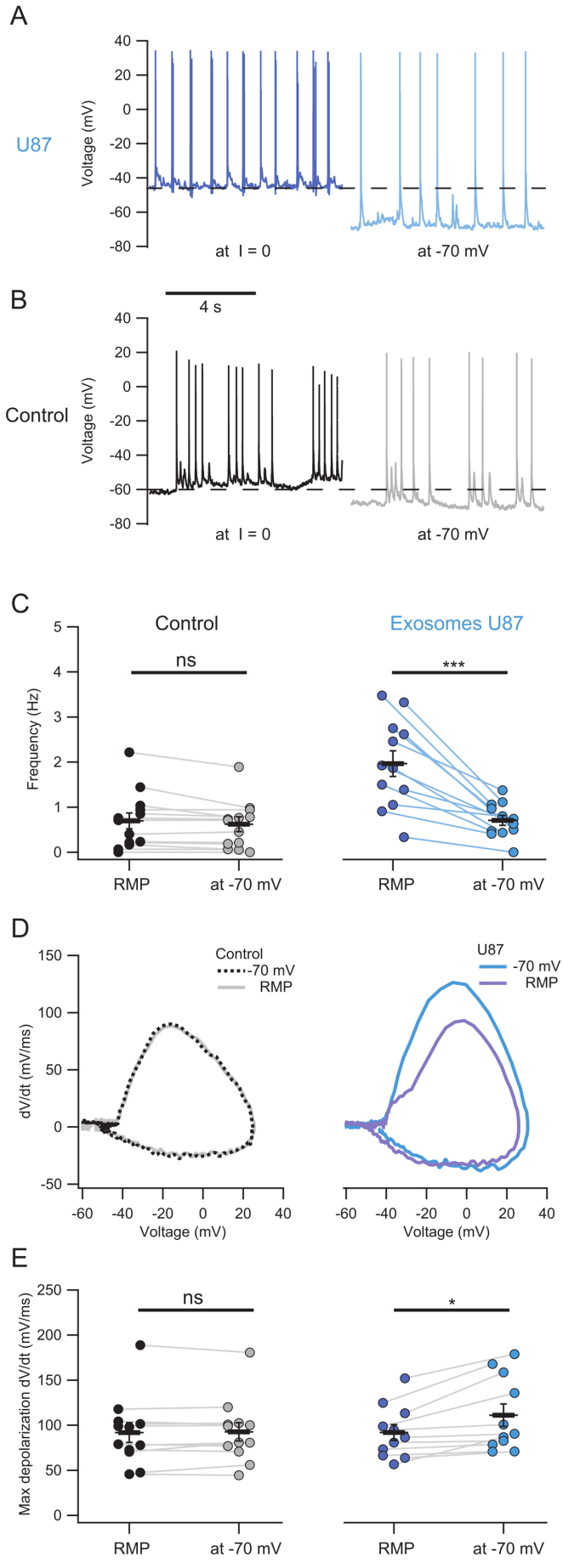
A
U87
Voltage (mV)
40
20
0
-20
-40
-60
-80
at I = 0
at -70 mV
B
4 s
Control
Voltage (mV)
40
20
0
-20
-40
-60
-80
at I = 0
at -70 mV
C
Control
Exosomes U87
ns
***
Frequency (Hz)
5
4
3
2
1
0
RMP
at -70 mV
RMP
at -70 mV
D
Control
-70 mV
RMP
U87
-70 mV
RMP
dV/dt (mV/ms)
150
100
50
0
-50
-60
-40
-20
0
20
40
Voltage (mV)
-60
-40
-20
0
20
40
Voltage (mV)
E
ns
*
Max depolarization dV/dt (mV/ms)
250
200
150
100
50
0
RMP
at -70 mV
RMP
at -70 mV

Figure 4: Exosomes increase excitability of hippocampal neurons, accelerating the depolarizing phase of action potential initiation. A. Representative traces of treated neurons recorded in current clamp (I=0) display a highly depolarized resting membrane potential (RMP, dark blue) and same cell held at -70 mV. **B.** Control neurons recorded as in A. **C.** Comparison of the spontaneous activity frequency of hippocampal neurons held at RMP (I=0) versus -70 mV. Control neurons had an average frequency of 0.69±0.18 Hz at RMP, with no significant change observed when hyperpolarized to -70 mV (0.62±0.16 Hz; ns, $p>0.05$, Wilcoxon paired samples test). In contrast, treated neurons decreased their spontaneous activity when an hyperpolarizing current was injected, reducing the frequency from 1.96±0.28 Hz at RMP to 0.7±0.11 Hz at -70 mV (**$p<0.01$, Wilcoxon paired samples test). **D-E.** Mean action potential phase plot shows increased maximum depolarization rate (dV/dt) when U87-exosomes treated neurons are held at -70 mV (111.1±12.4 mV/ms) compared to those at RMP (92±8.7 mV/ms; *$p<0.05$, Wilcoxon paired samples test). This effect is not observed in control neurons, which exhibit similar rates at both -70 mV (92.7 ± 10.08 mV/ms) and at RMP (91.8 ± 11 mV/ms, $p>0.05$, Wilcoxon paired samples test). In all panels, n=12 control, n=13 treated.

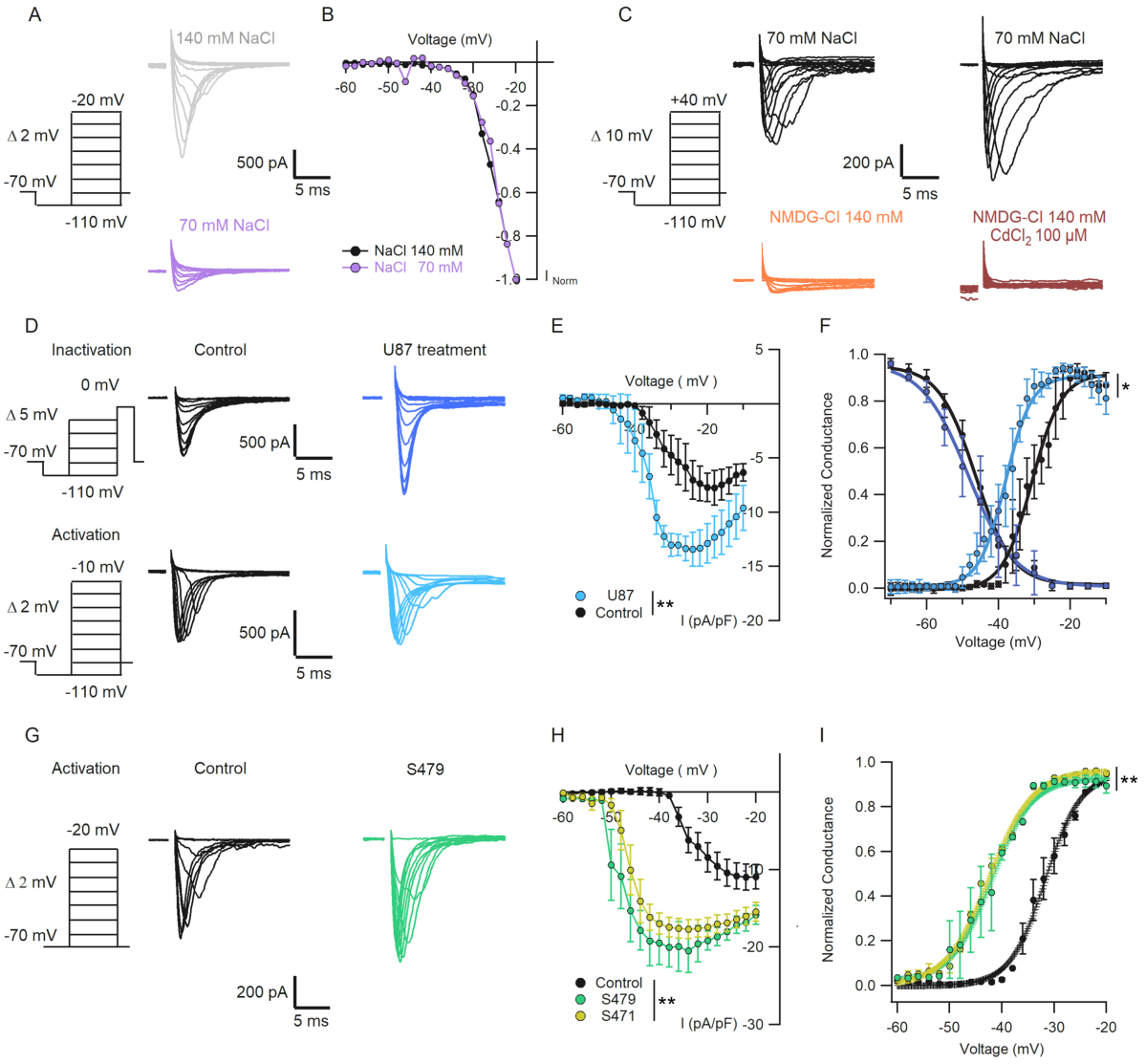

Figure 5: Increased spontaneous firing is associated to a shift of the activation curve of the inward voltage dependent Na^+ current. A. Representative traces of voltage-dependent Na^+ current activation in presence of 140 mM (gray) and 70 mM (purple) NaCl. **B.** Normalized currents in A shows a similar voltage activation dependence in the two groups, Kruskal-Wallis test, p>0.05; n=5. **C.** Complete replacement of NaCl by NMDG-Cl shows a residual small inward current (orange trace) blocked by addition of $CdCl_2$ 100 µM (brown trace); n=5. **D.** Representative traces of voltage-dependent Na^+ currents obtained with CdCl 100 µM in the extracellular solution and internal solution with CsCl 135 mM + NaCl 5 mM. Currents were recorded with the protocols used for activation and inactivation in control (black traces: n=7-10) and U87 exosomes (blue traces: n=12-14) treated neurons. **E.** I-V curve

comparing the current density as in D, showing increased current in treated neurons (Kruskal-Wallis test, **p<0.01). **F.** Dependence of the normalized conductance g/max g as a function of voltage for control and treated neurons, showing an average $V_{1/2}$ shift of -6.4 mV (values in main text, *p<0.05, Mann-Whitney-U test). **G.** Representative traces of Na^+ currents activated under control conditions (black traces, n=7) and in neurons treated for 24 h with exosomes from the patient S479 (green, n=7) **H.** Average I-V curves of Na^+ currents for control and patients' exosomes treated neurons, showing higher Na^+ current density in cells treated with patients' exosomes (Kruskal-Wallis test, **p<0.01). **I.** Normalized conductance curve for the conditions in H showing an early activation of the Na^+ conductance of neurons treated with patients' exosomes ($V_{1/2}$ Shift of -12±7.2 mV, values in main text, **p<0.01, Mann-Whitney-U test). Voltage clamp protocols used to test the activation and inactivation of the Na^+ current are shown on the right in each panel.

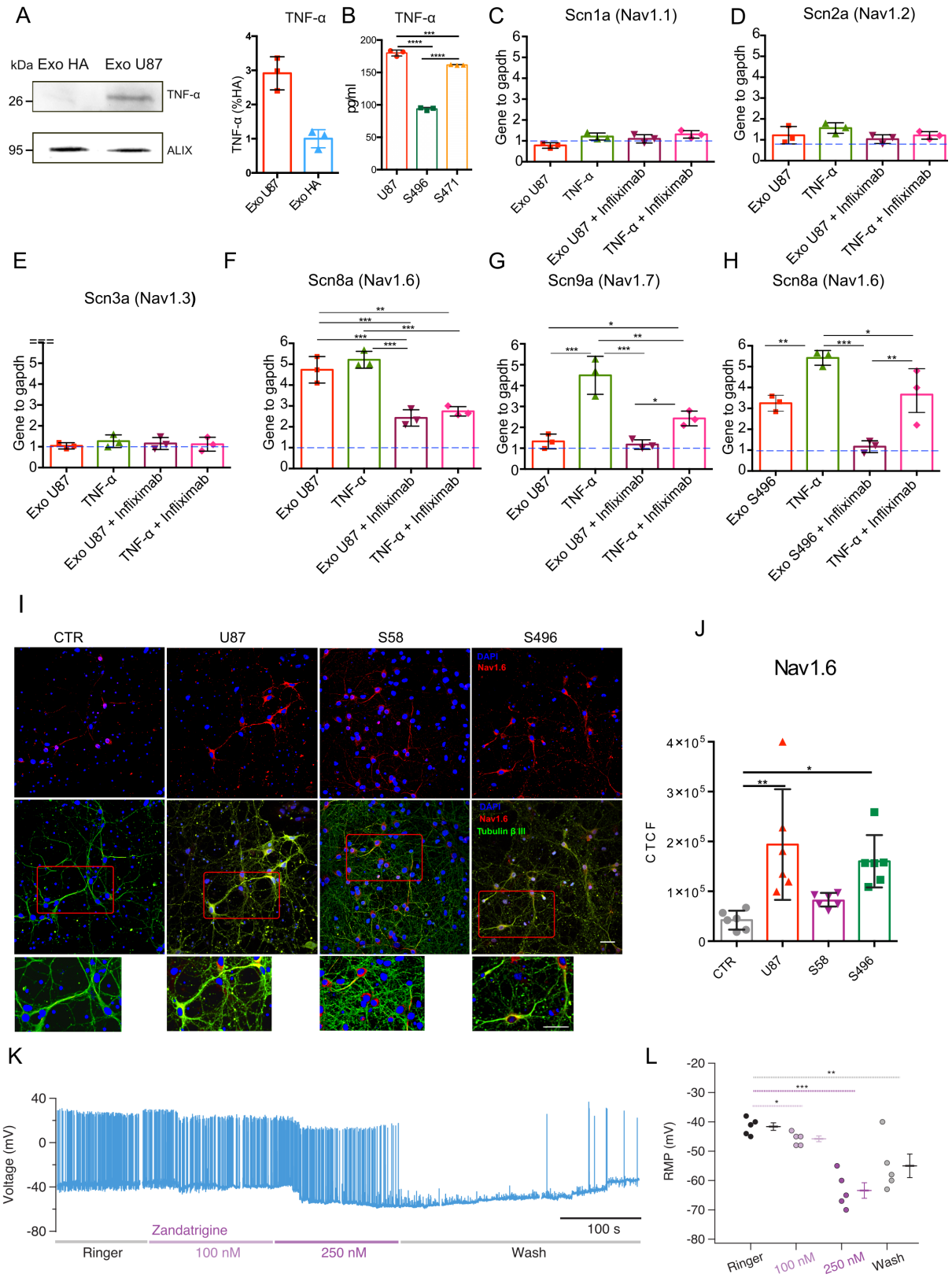

Figure 6: Exosomal TNF-α induces Nav1.6 overexpression. A. Lysates of HA and U87-exosomes were analyzed by SDS-PAGE followed by western blotting (left) using anti-TNF-α

and ALIX antibodies. Quantification of TNF-α (right) was obtained by normalization to the exosome marker ALIX and reported as percentage with respect to HA (n=3 exosome samples, two-tailed t test; ****p<0.01). **B.** Quantification of TNF-α in U87 exosomes and patients S496 and S471 using ELISA (n=3 independent cultures). **C-G.** RT- PCR quantification of Scn1a, Scn2a, Scn3a, Scn8a and Scn9a in hippocampal neurons treated with U87 exosomes (Exo U87), TNF-α, U87 exosomes plus Infliximab pre-treatment (Exo U87 + Infliximab) and TNF-α plus Infliximab pre-treatment (TNF-α + Infliximab). **H.** RT-PCR quantification of Scn8a using exosomes derived from patient S496 and the above-described conditions. The blue dashed line represents gene expression under control conditions, set to 1. Each gene is normalized on the housekeeping gapdh gene. (n=3 independent cultures). **I.** Primary hippocampal neurons were exposed to control (CTR), U87 (U87), patient S58 (S58) and S496 (S496) exosomes, fixed and stained with anti-Nav1.6 (red channel), anti-β-III tubulin (green channel) and DAPI to stain nuclei (blue channel). Scale bars: 50 μm. **J.** Quantification of the experiment in (I) reported as corrected total cell fluorescence (CTCF). n=6 coverslips from 2 independent dissections. Each point represents the average of four fields acquired for each coverslip. All data are shown as mean with standard deviation. One-way ANOVA followed by Dunnett's post-hoc test. (*p<0.05, **p<0.01, ***p<0.001, ****p<0.0001). **K.** Representative electrical recordings in current clamp mode (I=0) from a treated neuron in the presence of increasing amounts of the specific Nav1.6 blocker Zandatrigine. 250 nM Zandatrigine blocked the spontaneous AP firing and this effect was partially reversible following blocker removal. **L.** Quantification of the Zandatrigine effect on RMP. Kruskal-Wallis followed by Bonferroni corrected Dunn's test; *p<0.05, **p<0.01, ***p<0.001; n=5.

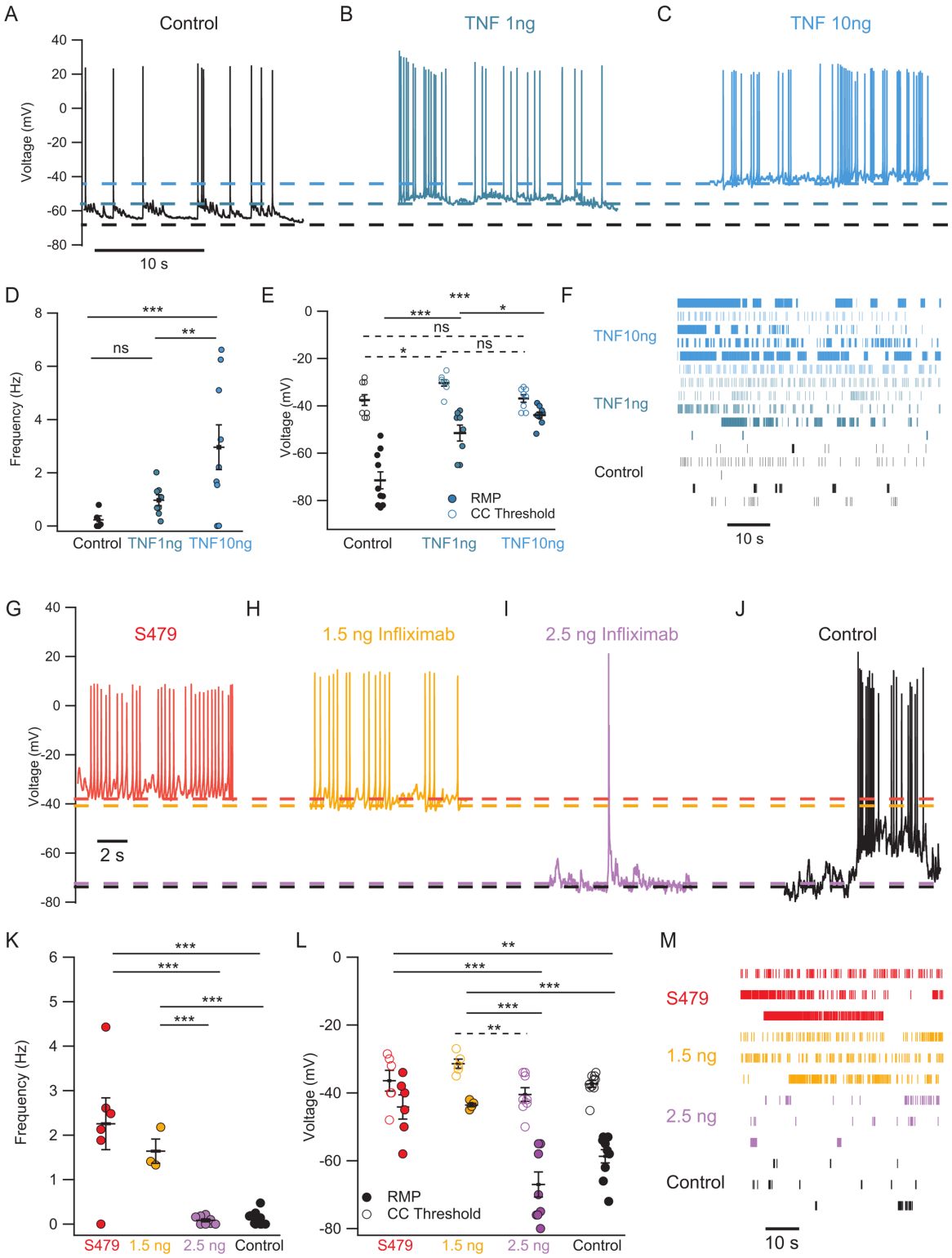

Figure 7: TNF-α depolarized RMP and increased firing frequency similar to exosomes, an effect that is antagonized by Infliximab. A-C. Representative current clamp traces under control conditions (black), in a neuron treated for 24 h with low (green) and high (blue) TNF-α concentration. **D-E**. Quantification of spontaneous firing frequency, RMP and AP threshold

for control neurons and those treated with low and high TNF-α concentration. Continuous line for RMP, dashed lines for threshold values. **F.** Raster plots of the firing in the three experimental conditions. **G-H.** Representative current clamp traces of a neuron treated with patient-derived exosomes (red, n=6) and neurons pre-treated with 1.5 ng/ml infliximab (yellow, n=3-5), both showing high spiking frequency. **I-J.** as in G and H but for control neurons (black, n=10) and neurons pre-treated with 2.5 ng/ml Infliximab before exosome application (purple, n=8). Dashed lines indicate AP threshold for the four experimental conditions. **K.** AP frequency for the groups in G-J. **L.** AP threshold (empty circles) and RMP (filled circles) for the treatments in G-J. 2.5 ng Infliximab decreased AP frequency and increased the difference between the RMP and AP threshold. **M.** Raster plots of the firing in the four experimental conditions. Control values: RMP=-58.7±2 mV; threshold=-37.4±1 mV. Kruskal-Wallis followed by Bonferroni corrected Dunn's test *** $p<0.001$, ** $p<0.01$, * $p<0.05$.